Article

Developmental Cell

A Temporal Transcriptional Switch Governs Stem Cell Division, Neuronal Numbers, and Maintenance of Differentiation

Highlights

- A *Drosophila* neural stem cell subtype transiently amplifies by symmetric division
- A temporal transcriptional switch defines the transition to transient amplification
- The transcriptional switch also programs maintenance of neuronal differentiation
- Failure of the transcriptional switch results in the loss of neurons

Authors

Natalia Mora, Carlos Oliva, Mark Fiers, ..., Annelies Claeys, Natalie De Geest, Bassem A. Hassan

Correspondence

natalia.moragarcia@icm-institute.org (N.M.), bassem.hassan@icm-institute.org (B.A.H.)

In Brief

Mora et al. discover neural stem cells in the *Drosophila* brain that divide symmetrically to double their numbers before generating one of the largest neuronal lineages in the fly. Atonal, the transcription factor that regulates stem cell doubling, also programs the maintenance of a differentiated state in their daughter neurons.

Mora et al., 2018, Developmental Cell *45*, 53–66
April 9, 2018
https://doi.org/10.1016/j.devcel.2018.02.023

CellPress

Developmental Cell
Article

A Temporal Transcriptional Switch Governs Stem Cell Division, Neuronal Numbers, and Maintenance of Differentiation

Natalia Mora,[1,2,3,*] Carlos Oliva,[2,3,4] Mark Fiers,[2,3] Radoslaw Ejsmont,[1,2] Alessia Soldano,[2,3,5] Ting-Ting Zhang,[1,3] Jiekun Yan,[2,3] Annelies Claeys,[2,3] Natalie De Geest,[2,3] and Bassem A. Hassan[1,3,6,*]
[1]Institut du Cerveau et de la Moelle Epinière (ICM) - Hôpital Pitié-Salpêtrière, Sorbonne Université, Inserm, CNRS, Paris, France
[2]VIB Center for the Biology of Disease, VIB, Leuven, Belgium
[3]Center for Human Genetics, University of Leuven School of Medicine, Leuven, Belgium
[4]Present address: Department of Cell and Molecular Biology, Faculty of Biological Sciences, Pontificia Universidad Católica de Chile, Alameda 340, Santiago, Chile
[5]Present address: Laboratory of Translational Genomics, Centre for Integrative Biology, University of Trento, Trento, Italy
[6]Lead Contact
*Correspondence: natalia.moragarcia@icm-institute.org (N.M.), bassem.hassan@icm-institute.org (B.A.H.)
https://doi.org/10.1016/j.devcel.2018.02.023

SUMMARY

The importance of producing the correct numbers of neurons during development is illustrated by both evolutionary enhancement of cognitive capacities in larger brains, and developmental disorders of brain size. In humans, increased neuronal numbers during development is speculated to partly derive from a unique subtype of neural stem cells (NSCs) that undergo a phase of expansion through symmetric self-amplifying divisions before generating neurons. Symmetric amplification also appears to underlie adult neural stem maintenance in the mouse. However, the mechanisms regulating this behavior are unclear. We report the discovery of self-amplifying NSCs in *Drosophila* and show that they arise by a spatiotemporal conversion of classical self-renewing NSCs. This conversion is regulated by a temporal transition in the expression of proneural transcription factors prior to cell division. We find a causal link between stem cell self-amplification and increased neuronal numbers. We further show that the temporal transcriptional switch controls both stem cell division and subsequent neuronal differentiation.

INTRODUCTION

The development of functional organs relies on the coordinated production of cells of different identities with temporal, spatial, and numerical precision. In the brain, where information processing depends on the output of interconnected neuronal circuits, not only the ratios of different neuronal subtypes, but also absolute numbers are important for optimal function. The number of neurons in the adult brain is a direct consequence of a spatiotemporally coordinated sequence of divisions of neural stem cells (NSCs) during development. However, it remains unclear how NSCs alter their division patterns over time and whether these alterations are causal to the generation of the correct number of neurons. Less clear still is whether and how the temporal transitions in NSC division influence the differentiation of their progeny.

In both mammals and insects NSCs regulate neurogenesis through a series of self-renewing divisions (Doe, 1996; Wodarz and Huttner, 2003; Zhong and Chia, 2008). NSC division patterns can be broadly classified in five categories. In three of these, NSCs divide asymmetrically renewing themselves and giving rise to daughters that differ in their proliferation potentials: daughters that do not divide, daughters that divide once, and daughters that divide multiple times (Baumgardt et al., 2014; Bello et al., 2008; Boone and Doe, 2008; Taverna et al., 2014). In the other two, NSCs divide symmetrically. One type of symmetric division common to vertebrates and invertebrates signals the end of stemness through the generation of two daughter cells committed to differentiation (Maurange et al., 2008). A second, much rarer type, expands the progenitor pool through the generation of two cells, which retain the expression of NSC markers and the ability to generate neurons. In mouse, self-renewal by symmetric division has recently been reported to be predominant during adult neurogenesis (Obernier et al., 2018), in contrast to what is observed in embryonic stages where most NSCs divide asymmetrically (Miyata et al., 2001; Noctor et al., 2004). In the primate brain, embryonic self-amplifying divisions have been detected in the NSCs known as outer radial glia (oRG) (Hansen et al., 2010; Lui et al., 2011). Multiple lines of evidence support the hypothesis that oRGs' high abundance and proliferative capacity are critical for the vast increase of brain size in primates (Reillo and Borrell, 2012; Stahl et al., 2013). However, the direct evidence for the impact of symmetric amplification of NSCs on neuronal numbers, the mechanisms that mediate the switch from self-renewal to self-amplification and then to neurogenesis, and the impact of such a switch on terminal differentiation remain unexplored.

The fruit fly *Drosophila melanogaster* has long been a powerful model system for the discovery of the genetic, cellular, and

molecular underpinnings of the behavior of NSCs, as well as the generation and differentiation of their neuronal progeny (Doe et al., 1998; Li et al., 2014; Wodarz and Huttner, 2003). *Drosophila* NSCs are called neuroblasts (Nbs), and two major modes of neurogenesis have been described (Baumgardt et al., 2014; Bello et al., 2008; Boone and Doe, 2008; Maurange et al., 2008). The type I Nbs self-renew while giving rise to committed daughters called ganglion mother cells (GMCs) that in turn divide terminally to produce two neurons or glia. The type II Nbs also self-renew but produce intermediate progenitors that in turn undergo a limited number of self-renewing divisions giving rise to GMCs, which give rise to neurons. Thus, to date, all Nbs in the fly brain are thought to produce neurons by asymmetric self-renewal and no symmetrically dividing, self-amplifying, NSCs have been found.

The majority of the fly brain is dedicated to visual processing. The higher-order visual centers called the optic lobes (OLs) receive the visual input from the retina and are arranged in four neuropils called lamina, medulla, lobula, and lobula plate (LP); all four organized in retinotopic maps (Nériec and Desplan, 2016). OL neurons derive from two major proliferation zones, called the outer proliferation center and the inner proliferation center (IPC), containing actively dividing Nbs. The organization of the OLs is constrained by the characteristics of the compound eye, which is composed of ~750 repetitive units of 8 photoreceptors covering the visual field and projecting to the OL in a retinotopic order. This integration of the retinal map requires a tight control of the diversity and stoichiometry of the neuronal populations. While temporal and spatial cues required to generate different types of neurons have been identified (Allan and Thor, 2015; Erclik et al., 2017), the control of the production of large numbers of neurons is much less understood. One striking example is the motion detection neurons of the LP called T4/T5. For each of the 750 retinal units, the LP contains 8 different T4/T5 direction sensitive neurons (T4a, b, c, d, and T5a, b, c, d, respectively) (Behnia and Desplan, 2015; Borst and Helmstaedter, 2015; Takemura et al., 2017). Thus, the direction-selective T4/T5 lineage generates approximately 12,000 neurons—representing more than 10% of all neurons in the fly brain. How such a massive proportion of neurons is generated is entirely unknown.

Another highly conserved feature of neurogenesis is that it is regulated by a small and highly conserved set of transcription factors known as the proneural proteins. First described in *Drosophila*, basic loop-helix proneural factors regulate neurogenesis in insects as well as in mammals (Bertrand et al., 2002; Huang et al., 2014; Kiefer et al., 2005). There are three families of proneural proteins named after their founding members; the Atonal (ATH), Achaete-scute (AS), and Neurogenin families. Proneural proteins most conserved function is to provide progenitors with the neuronal fate (Bertrand et al., 2002). In addition, they have been found to promote asymmetric division, exit from cell cycle and initiation of differentiation (Guillemot and Hassan, 2017). Whether proneural proteins can promote symmetric proliferation or if they can combine their proliferation and differentiation functions in the same neuronal linage is still unclear.

Here we identify the first symmetrically self-amplifying NSCs in *Drosophila* giving rise to the population of T4/T5 neurons. We show that these Nbs are generated by a temporal conversion of asymmetrically dividing Nbs, which is accompanied by a temporal transition in proneural protein expression from the AS protein Asense (Ase) to the ATH protein Atonal (Ato). Furthermore, we discover that the switch from Ase to Ato is necessary and sufficient for the switch in stem cell division pattern and the generation of the correct number of neurons. Lastly, we demonstrate that Atonal creates a quantitative change in target gene expression that is propagated throughout the lineage to ensure the commitment of T4/T5 neurons to terminal differentiation.

RESULTS

Drosophila OL IPC Nbs Undergo a Spatiotemporal Transition

In the developing fly brain, a region known as the IPC gives rise to two different types of neurons known as C/T and T4/T5 neurons (Figure 1A). In a first phase, soon after larval hatching, the IPC primordium proliferates symmetrically, expanding the pool of neuroepithelial (NE) progenitors (Egger et al., 2007; Hofbauer and Campos-Ortega, 1990; Ngo et al., 2010). During a second phase, halfway through the larval period, the progenitors undergo an epithelial-to-mesenchymal transition and migrate along the proximo-distal axis in four main streams connecting the NE with the Nbs cluster (Apitz and Salecker, 2015, Figure 1A). Progressively, all NE cells mature into Nbs in a process that lasts until early pupal stages when the NE is no longer visible (Ngo et al., 2017). The continuous arrival of new progenitors to the Nb cluster creates a gradient of Nbs that are at different developmental stages along the proximo-distal axis. At lower positions, and therefore early stages, IPC Nbs generate C/T neurons, while at upper positions, and therefore later stages, the Nbs switch to the production of T4/T5 neurons that expressed the POU domain protein Acj6 (Figures 1A and S1). The two temporal phases are characterized by the expression of two proneural proteins expressed in complementary patterns: Ase at lower/early and Ato at upper/late stages (Figures 1B and 1C). The latter is co-expressed with the retinal determination gene Dachshund (Figures 1A and S1). For simplicity, in the rest of the study we refer to the early stage, proximally located, Nbs that express Ase as "lower-Nbs" and to the later stage, distally located, Nbs that express Ato as "upper-Nbs."

In agreement with the sequential expression of Ase and Ato we observed that if we follow the lineage of lower-Nbs with an *ase*-gal4 driving the expression of GFP, all the Dpn+ Nbs, both lower and upper, express GFP (Figure 1D). In addition, T4/T5 neurons (Acj6+) also retain GFP expression, indicating that *ase*-Gal4 labels the entire IPC lineage. In contrast, if we follow the lineage of upper-Nbs with an *ato*-lacZ lineage tracer, only upper-Nbs and their T4/T5 progeny are positive for β-gal (Figures 1E–1J). Using this differential expression of *ato*-driven β-gal we describe the characteristic spatial organization of the two lineages. GMCs (Pros+, β-gal−) and neurons (Elav+, β-gal−) produced by lower-Nbs (Dpn+, β-gal−) are organized in rings surrounding the lower-Nb cluster (Figures 1E–1G). On the other hand, GMCs (Pros+, β-gal+) from upper-Nbs (Dpn+, β-gal+) are found in an internal ring intermingled with upper-Nbs, while their daughters, the T4/T5 neurons (Elav+, β-gal+), are clustered in the center of the u-shaped Nbs domain (Figures 1H–1J). Direct evidence that the switch from Ase to Ato expression is a temporal

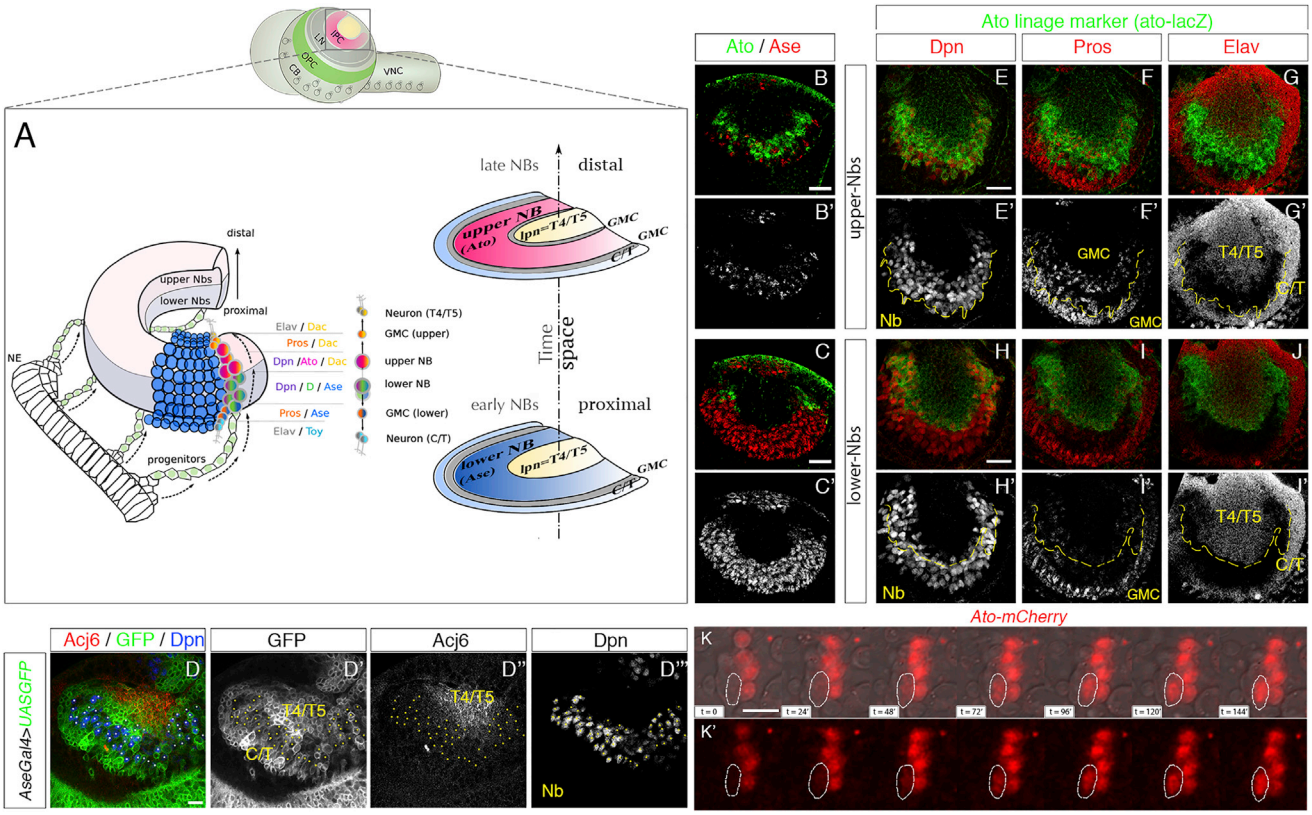

Figure 1. Temporal Transition at the IPC

(A) Schematic representation of the development of C/T and T4/T5 neurons at the IPC. NE, neuroepithelium; Nbs, neuroblast; GMC, ganglion mother cell. NE cells migrate in columns to form the Nbs cluster. First IPC Nbs generate C/T and later T4/T5. The continuous arrival of NE forms a gradient of young lower-Nb that produce C/T neurons and old upper-Nbs that produce T4/T5 neurons. Cell-type markers and a scheme of the organization of the IPC in lateral sections.

(B and C) Expression pattern of Ase (red) and Ato (green) at lower (C) and upper (B) positions. (B' and C') Ase single channel.

(D) Co-localization of GFP (green) driven by Ase-Gal4, Acj6 (red), and Dpn (blue). Dots, Dpn+ cells.

(E–J) Co-expression of the ato-linage tracer ato-lacZ (green) with Dpn (E and H), Pros (F and I), and Elav (G and J) (red) at lower (H–J) and upper (E–G) positions. Single channels of Dpn (E' and H''), Pros (F' and I'), and Elav (G' and J'). Yellow line, contour of ato-lacZ expression.

(K) Life imaging of primary cultures from L3 brain disaggregates showing the expression of ato over time. Brightfield (gray), ato (red) (K and K'). White circle identifies the same cell over time.

Scale bars, 10 μm. See also Figure S1 and Movie S1.

transition of the same Nbs comes from live imaging of primary cultures of L3 Nbs from animals in which we used the IMAGO homologous recombination approach (Choi et al., 2009) to replace the *ato* open reading frame by an *ato* tagged with mCherry, which mimics the expression of endogenous Ato (Weinberger et al., 2017). We find that Ato-mCherry accumulates over time without detectable cell division (Figure 1K; Movie S1).

Altogether, our data support the current model in which IPC Nbs produce first C/T and then T4/T5 neurons in a birth order-dependent manner coinciding with the sequential expression of Ase and Ato. Interestingly, the progression in the type of neurons does not depend on the switch from Ase to Ato expression (Oliva et al., 2014; Apitz and Salecker, 2015), and the role of the proneural switch is unknown.

Upper-Nbs Self-Amplify by Symmetric Division

T4/T5 LP neurons constitute one of the largest neuronal populations in the *Drosophila* brain. While there are approximately twelve thousand T4/T5 neurons, C/T neurons produced from the same Nbs at earlier stages are two times less numerous (Takemura et al., 2008). We asked whether this temporal difference in lineage stoichiometry might be linked to changes in NSC division behavior. To this end, we performed *in vivo* live imaging on brain explants of L3 larvae in which the Nb marker Dpn is endogenously tagged with GFP, and the entire upper-Nb lineage is marked with a fluorescent Ato lineage tracer line (IPC-5x mCherry) generated for this study (see the STAR Methods). Time-lapse movies of upper-Nbs (Dpn+, IPC-Cherry+) show an atypical mitosis that is symmetric in size and Dpn distribution (Figure 2A; Movie S2). We find that Dpn is retained in the nucleus of the two daughters after the division, suggesting that an upper-Nb divides to give rise to two other Dpn+ upper-Nbs, thus undergoing an amplifying division. Furthermore, all 65 divisions we followed over the course of 13 hr were symmetric, illustrating that amplifying divisions are highly frequent. In fixed samples we consistently find a 2-fold increase in the number of upper-Nbs compared with lower-Nbs, further supporting a symmetric amplification (Figures S2A and S2B).

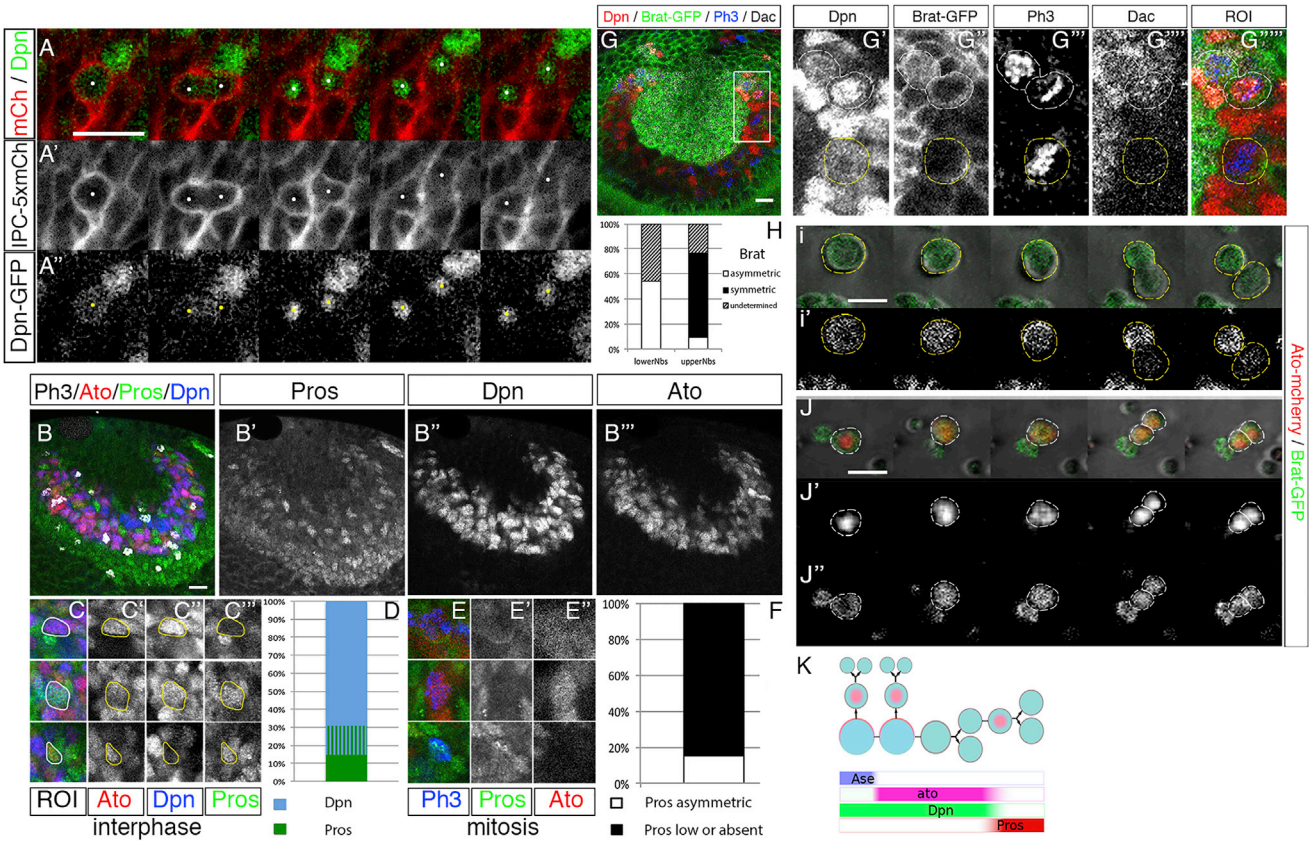

Figure 2. Transient Amplification by Symmetric Division of Upper-Nbs

(A–A'') Live imaging of L3 brain explants showing upper-Nbs lineage (red) and Nbs (green). Dots mark an upper-Nbs undergoing symmetric division.

(B–F) Characterization of Ato+ cells at interphase and mitosis. (B) Co-localization of ato (red) with Pros (green), Dpn (blue), and ph3 (gray). (C) Magnification of Ato+ cells (red) at interphase (Ph3−) showing three different patterns of co-localization with Dpn (blue) and Pros (green): Ato-Dpn (upper panel), Ato-Dpn-Pros (middle panel), and Ato-Pros (lower panel). (D) Quantification of the frequency of each of the three patterns (n = 358 cells from two samples). (E) Magnification of Ato+ cells (red) in mitosis (ph3+, blue) showing two patterns of Pros (green) localization: Pros asymmetric in the cortex (upper panel) and Pros low or absent in the cytoplasm (middle panel). Lower panel shows the Pros nuclear localization in GMC that we never observed in ato+ cells. (F) Quantification of the frequency of each of the two Pros patterns in mitotic Ato+ cells (n = 58 mitosis from five samples).

(G–J) Brat during mitosis in IPC Nbs. (G) Localization of Brat-GFP (green) during mitosis in lower-Nbs stained with Dpn (red) and upper-Nbs stained with Dpn (red), and Dachshund (Dac) (gray). Mitosis are stained with Ph3 (blue). Left panels: magnifications of square: yellow circles, lower-Nb; white circles, upper-Nbs. (>) Brat asymmetric accumulation. (H) Quantification of the frequency of Brat asymmetric or symmetric localization in upper and lower-Nbs. When the pattern was not clear the mitosis was labeled as undermined (n = 81 mitosis from two samples). (I and J) Live imaging of primary cultures from L3 brain disaggregates showing brightfield (gray), Brat (green), and ato (red). Yellow circles, ato– Nb; white circles, ato+ Nb. (>) Asymmetric accumulation of Brat.

(K) Working model of the transitions based on the results of the figure.

Scale bars, 10 μm. See also Figure S2 and Movies S2 and S3.

In classic Nbs, the Pros protein is asymmetrically tethered to the membrane during mitosis and is inherited by the GMCs where it translocates to the nucleus to promote cell-cycle exit and terminal differentiation. The only exception to this rule is the final symmetric division where Pros moves into the nucleus of the terminal Nb itself signaling the end of the Nbs life (Maurange et al., 2008). To further study the nature of upper-Nbs divisions we analyzed the localization of the Pros protein at interphase and during mitosis. We find three categories of cells in interphase. Of all Ato+ cells, 70% express Dpn but not Pros (Figures 2B and 2C), 14% express both Dpn and Pros, and 16% express Pros, but not Dpn, indicating the presence of a small number of terminal Nbs and/or GMCs in which Ato expression persists. More importantly, 85% of all mitotic Ato+ cells show either absent or, occasionally, weak cytoplasmic Pros (Figure 2E). The remaining 15% localize Pros asymmetrically at the membrane, indicating residual asymmetric divisions in upper-Nbs (Figure 2E). In summary, in agreement with the live-imaging observations, these data show that the vast majority of upper-Nbs divide symmetrically in the absence of Pros, producing two Nbs from one.

A typical marker of asymmetric division in fly Nbs is the protein Miranda (Mira), which is required to tether Pros to one end of the mitotic Nb during asymmetric division. We therefore examined Mira expression in mitotic lower- and upper-Nbs. In lower-Nbs, as expected, Mira is localized asymmetrically during mitosis (Figure S2C, arrows). In contrast, and correlating with the absence of Pros expression in most mitotic upper-Nbs, we find

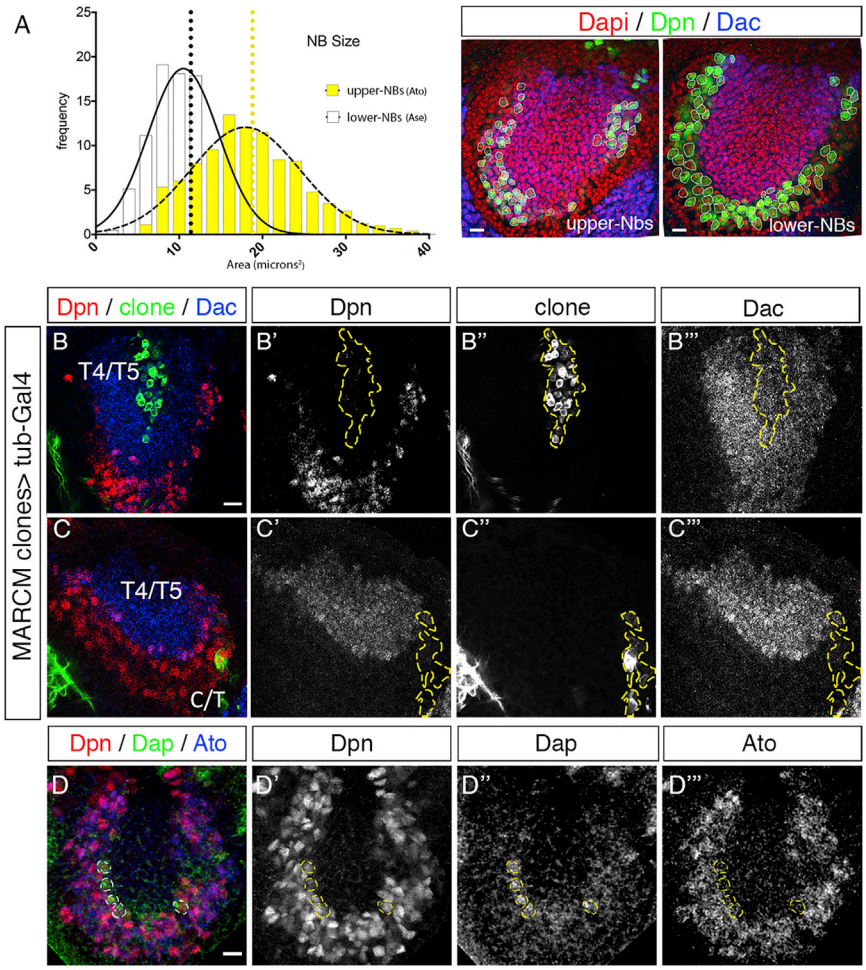

Figure 3. Cell-Cycle Exit Follows Transient Amplification

(A) Measures of nuclear size of lower (yellow, n = 771) and upper (white, n = 878) Nbs. Doted lines, mean values. $p < 0.0001$. On the right, example of white pupae IPC where we measured the size of lower-Nbs Dpn+ (green) and upper-Nbs Dpn+, Dac+ (blue). The nucleus are in red marked with DAPI.

(B and C) Linage content of wild-type MARCM clones. Clones are GFP+ (green), which is driven by the ubiquitous driver tub-gal4. Lower-Nbs Dpn+ (red), upper-NBs Dpn+ (red), and Dac+ (blue). Yellow dotted line, contour of the clone.

(D) Expression of the cell-cycle exit marker Dacapo (Dap) (green). Dpn is in red and Ato is in blue. Yellow line, contour of Dap+ cells.

Scale bars, 10 μm.

that upper-Nbs express low, diffused levels of Mira in ~85% of the cells examined (Figures S2C, S2D upper panels, and S2E) Also, like Pros, in ~15% of the cells, Mira is localized asymmetrically (Figures S2C, S2D lower panels, and S2E).

In addition to Pros and Mira, the repressor of translation Brain Tumor (Brat) is localized asymmetrically during the mitosis of classic Nbs. We therefore examined Brat localization in mitotic lower- and upper-Nbs. In lower-Nbs, whenever Brat was found at the membrane (55% of the cells examined) it was asymmetrically localized. In contrast, Brat is symmetrically localized at the membrane of the majority (70%) of mitotic upper-Nbs (Figures 2G and 2H). To ascertain that this symmetric localization in fixed tissue reflects symmetric inheritance of Brat, we performed live imaging of Nb cultures from Ato-mCherry larval brains also expressing Brat-GFP. The symmetric localization and inheritance of Brat in Ato+ upper-Nbs is striking, especially when compared with classic Nbs (Figures 2I and 2J; Movie S3). Finally, we compared the localization of overexpressed Numb-GFP (Figures S2F and S2G), an established marker of asymmetric division, in mitotic lower- versus upper-Nbs. Consistent with the behavior of Brat, Numb-GFP is asymmetrically localized in lower-Nbs (Figure S2G, yellow dashed circle) and symmetrically localized in upper-Nbs (Figure S2F, white dashed circle). Together our results provide strong evidence that upper-Nbs expand through a symmetric amplifying division. We refer to these previously undescribed symmetrically amplifying Nbs as type III Nbs (Figure 2K).

Cell-Cycle Exit Follows Transient Amplification

If Nbs divide symmetrically to generate more Nbs, how does the transition to neurogenesis occur? The presence of nuclear Pros in some of the upper-Nbs suggests that the amplification is transient and is followed by cell-cycle exit. One of the hallmarks of the exit of stemness is the reduction of Nb size (Fuse et al., 2003). During our live-imaging experiments, we noted a difference in cell size between upper- and lower-Nbs, suggesting that symmetric division is not followed by cell growth. To quantify this effect, we measured the nuclear sizes of lower- versus upper-Nbs and found a 1.6-fold difference in nuclear area (Figure 3A). To directly test whether upper-Nbs generate T4/T5 neurons via a terminal symmetric division following transient Nb amplification, we used mosaic analysis with a repressible cellular marker (MARCM) for lineage tracing (Lee et al., 2000). MARCM clones of asymmetrically self-renewing Nbs always contain the Nb within the clone. In contrast we find MARCM clones that contain T4/T5 neurons but are devoid of progenitors, as would be expected if these progenitors are consumed by symmetric divisions (Figure 3B). In contrast, we observe small clones that contain C/T neurons as well as lower-Nbs, consistent with the self-renewal of these Nbs (Figure 3C) and the sequential order in the production of C/T followed by T4/T5 neurons. To further confirm that Ato+ upper-Nbs undergo a terminal division after they amplify, we examined the expression of the *Drosophila* homolog of the P21 cyclin-dependent kinase inhibitor Dacapo (Dap) which is expressed in terminally dividing cells (Lane et al., 1996). We find that Dap is expressed in few upper-Nbs (Dpn+, Ato+) at the border between the u-shaped cluster of Nbs and the nascent T4/T5 cluster (Figure 3D), indicating that these Nbs are entering their last cell cycle.

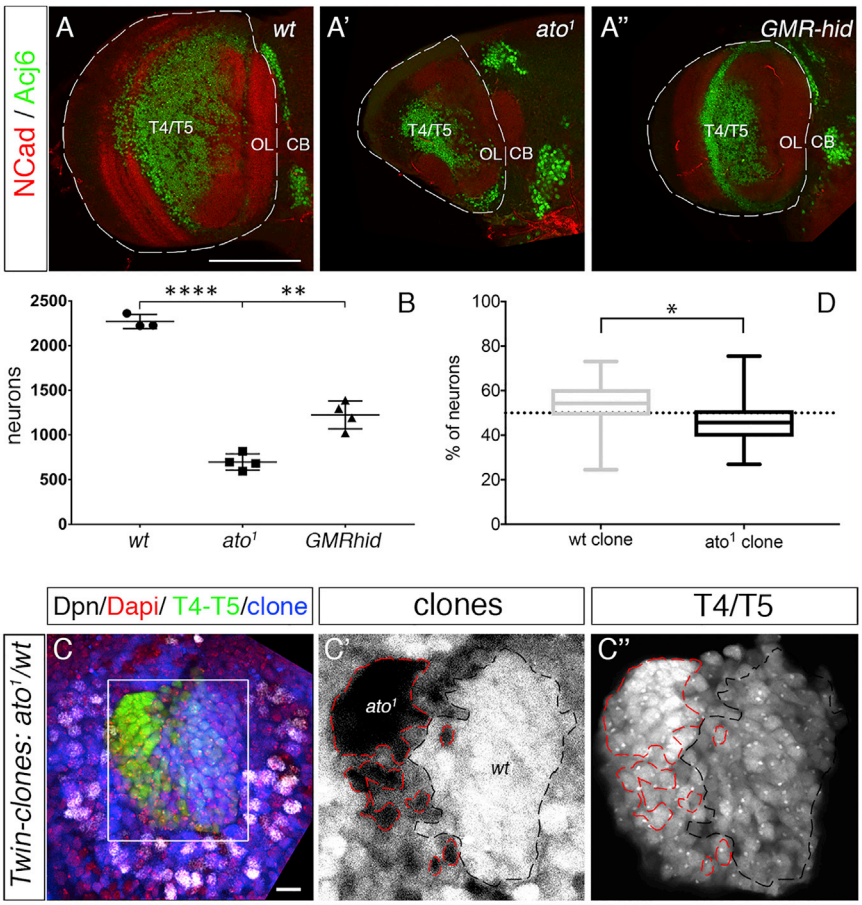

Figure 4. Ato Control of T4/T5 Numbers

(A and B) Ato control of the number of adult T4/T5 neurons. (A–A''). Localization of the T4/T5 marker Acj6 (green) and Ncad (red) in adult optic lobes of *wt*, *ato*^{1}, and *GMR-hid* flies. Dotted line indicates contour of optic lobes. Scale bar, 100 μm. (B) Number of T4/T5 Acj6+ neurons per genotype (number of optic lobes used in: *wt* = 3; *ato*^{1} = 4; *GMR-hid* = 4. Statistical test: unpaired Student's t test).

(C–D) Comparison of *wt* and *ato*^{1} twin clones. Clones (blue) (single channel in C') are labeled by RFP, T4/T5 neurons (green) (single channel in C'') are labeled by GFP driven by IPC-Gal4, Nbs are labeled with Dpn (gray), and nuclei are labeled with DAPI (red). Intermediate intensities of the clone reporter (blue) correspond to the heterozygote background *ato*^{1}/*wt*. Intense reporter expression corresponds to the *wt* clone (black dotted line). Absence of clone reporter corresponds to the *ato*^{1} mutant clone (red dotted line). Scale bars, 10 μm. (D) Comparison of the percentage of neurons that are *wt* versus *ato*^{1} mutant in 32 optic lobes. (Mean values: 53,23 in *wt* clone, 46,75 in *ato*^{1} mutant clone. p = 0.0206. Paired Student's t test).

*p < 0.05, **p < 0.005, ****p < 0.00005. See also Figure S3.

Altogether, our data show that upper-Nbs undergo a transient amplification prior to cell-cycle exit.

The Transition from Ase to Ato Regulates the Onset of Transient Amplification

Why IPC Nbs undergo a temporal transition in proneural protein expression from Ase to Ato is unknown. To address this issue, we first examined the function of Ato in T4/T5 lineage development. In null *ato* mutants the size of the LP, where T4/T5 neurons reside, is markedly reduced. However, loss of Ato function also results in the complete loss of the retina (Jarman et al., 1994) and the subsequent loss of major parts of the visual system. To control for potential indirect effects on T4/T5 development, we also examined flies in which the retina was genetically ablated using the *GMR-hid* flies. We quantified the number of T4/T5 Acj6+ cells in the LP of *wild-type (wt)*, *GMR-hid*, and *ato* null adult animals. We observe a 3.2-fold reduction in the number of nuclei expressing Acj6 in *ato* null mutants compared with *wt* (Figure 4A, A' and A'''). Quantification of Acj6 expression in *GMR-hid* flies shows that ~45% of this reduction is due to the loss of the retina, while the other 55% is due to lack of Ato function in the IPC (Figure 4B). To confirm these data independently of Acj6 expression, we attempted to generate flies where T4/T5 are marked by the ato *IPC-Gal4* driving the expression of GFP (*IPC-Gal4>GFP*; Oliva et al., 2014) in an *ato* null and *GMR-hid* backgrounds, respectively. Quantification of the number of GFP-positive cells shows a ~4-fold reduction in T4/T5 neurons compared with *GMR-hid*, *IPC-Gal4>GFP* controls (Figures S3A and S3B), confirming the reduction observed with Acj6 as a marker. Finally, we asked if this effect has a developmental origin. To this end, we generated twin *ato*^{1} null and *wt* clones, and analyzed the number of T4/T5 neurons at L3 stages (Figures 4C and 4D). The normalized comparison of 32 twin clones (58,298 neurons counted) shows a significant (p = 0.02) reduction of approximately 12% fewer neurons in *ato* null mutants compared with *wt* clones (Figure 4D). Although this is a relatively modest reduction, it is important to note that twin clones in the IPC can originate from any IPC progenitor, including the neuroepithelium, which is present until pupal stages, the asymmetric lower-Nbs, the symmetric upper-Nbs, and GMCs, or any combination thereof. Moreover, cell divisions in the IPC are not synchronized and far from being finished at L3 stages. To control for this inherent variability in the experiment, we performed an unpaired comparison of the *wt* and *ato*^{1} mutant clones from the 32 brains and find that they show no difference in distribution (Figure S3C). Next, we performed paired comparisons and found that *ato*^{1} mutant clones are on average 160 neurons smaller than their *wt* twins at L3 stages (Figure S3D). Altogether, these data support the developmental origin of the reduction in the number of T4/T5 neurons that we observe in *ato*^{1} mutant adults.

Next, we asked whether the proneural transition is causal to the switch in cell division and thus the generation of a large number of neurons. To answer this question, we examined the localization of cortical Mira in *ato* mutant Nbs. We observed that, in lower-Nbs, which do not yet express Ato, Mira is asymmetric

as it is in *wt* brains. In upper-Nbs, where Mira is normally low and diffused under *wt* (Ato+) conditions we observe a significant increase in the number of asymmetric Mira localization (15% *wt* versus 30% *ato*^{1}, Figures 5A and 5B). Then, we expressed Ato prematurely in lower-Nbs (Ase+) using overexpression clones and characterized the mode of division using the cortical localization of the Brat-GFP endogenous transgene during mitosis (Figure 5C). We find that Ato is sufficient to alter the mode of division of lower-Nbs, which, in approximately 70% of cases, show symmetric localization of Brat-GFP compared with 25% in *wt* (Figure 5D).

In addition to the switch in division mode, the onset of Ato expression and symmetric division of upper-Nbs is accompanied by a reduction in cell size (Figure 3A). We studied the size of upper-Nbs in *wt* and *ato* null mutants. We observed that upper-Nbs are larger and show a broader size distribution (Figure 5E) in *ato* mutants. Reciprocally, premature Ato expression in clones of lower-Nbs is sufficient to reduce their size compared with their *wt* neighbors (Figure 4F).

Interestingly, we also noted that Ase levels are reduced when Ato is prematurely expressed in lower-Nbs (14% reduction, $p < 0.0006$). To test if Ase downregulation is required for the Ato-induced transformation of lower-Nbs we overexpressed both Ato and Ase in lower-Nbs at the same time and examined the cortical localization of Mira during mitosis (Figure 5G). The quantification of asymmetric versus symmetric divisions shows that restoring high levels of Ase in clones expressing Ato prematurely rescues asymmetric division in lower-Nbs (Figure 5H). Finally, we overexpressed Ase at later stages in upper-Nbs and examined the localization of Brat (Figure 5I). We find that late Ase overexpression after Nbs have switched to Ato has no effect on their mode of division (Figure 5J). Therefore, at the early phase of the temporal proneural switch, high levels of Ase expression are required for asymmetric division. Once Nbs switch from Ase to Ato, they are committed to symmetric amplification and are no longer responsive to Ase.

In sum, our experiments provide compelling evidence that the temporal transition in proneural protein expression from Ase to Ato regulates the timing of onset of NSC transient amplification through symmetric division in the fly visual system. Furthermore, the onset of Ato expression defines a critical window where IPC Nbs switch their division mode and can no longer revert to asymmetric division.

Ato Schedules Differentiation of T4/T5 Neurons

Previous analyses have shown that, in the absence of Ato, the T4/T5 neurons that are produced displayed connectivity defects (Oliva et al., 2014). This is puzzling because Ato is exclusively expressed in upper-Nbs, but not in neurons (Figure S1B). Thus, while they themselves do not express Ato, T4/T5 neurons may require its activity in their progenitors. To investigate whether Ato schedules T4/T5 differentiation we examined the ribosome-bound mRNAs of T4/T5 neurons in *wt* versus *ato* null mutants using the TRAP technique (Thomas et al., 2012). Gene ontology analysis of the differentially expressed genes in *ato* null compared with the *wt* shows strong downregulation of gene ontology terms involved in neuronal differentiation such as "neuron development" or "neuroblast differentiation and neurotransmission" (Figure 6A). These data suggest that most, if not all, T4/T5 neurons derived from mutant upper-Nbs display at least some degree of lack of differentiation.

While analyzing *ato* null mutant brains with various markers, we noted the presence of cells ectopically expressing Nb markers in the region where normally only postmitotic T4/T5 neurons reside. To confirm these observations, we examined the expression of the Nb markers Dpn and Mira in *ato* null brains, where the entire T4/T5 lineage is marked with GFP (*IPC-Gal4>GFP*; Oliva et al., 2014). These analyses show Dpn+ and Mira+ cells in the T4/T5 zone (GFP+) (Figure 6B). To test if the expression of Nb markers in the neuronal compartment is due to an aberrant differentiation of T4/T5 or to the ectopic migration of some upper-Nbs into the T4/T5 cluster, we generated *ato* null MARCM clones in which upper-Nbs and their progeny are labeled with GFP. The progeny of *ato* null upper-Nbs in the MARCM clones contained cells expressing Dpn. The ectopic Dpn+ cells were never observed to be isolated from the clone, showing that they are indeed products of upper-Nb divisions rather than isolated Nbs (Figure 6C). In addition to Dpn, Ase and Mira are also miss-expressed in *ato* null mutant clones. Pros, on the other hand, is never detected, while the T4/T5 neuronal marker Acj6 is sometimes absent but more often reduced (Figures 6C–6F; Table S1). These data suggest that some T4/T5 neurons derived from *ato* mutant upper-Nbs revert to a stem cell-like phenotype. To ascertain the neuronal identity of cells with ectopic Dpn expression, we generated *ato* null MARCM clones using the postmitotic T4/T5 driver *Acj6-Gal4*. GFP driven by *Acj6-Gal4* labels exclusively the neuronal progeny of the MARCM clones, where once again we detect Dpn+ cells. Their morphology, especially the presence of neurites, further supports the neuronal identity (Figure 6D). It should be noted that even cells that show no Acj6 protein expression are marked with Acj6-gal4>GFP, which suggests that the expression from the locus is initiated, but later the protein is lost.

All together, these results demonstrate that Ato, despite being expressed only in upper-Nbs, is important for the differentiation of T4/T5 neurons and that the lack of Ato causes neuronal dedifferentiation to the point of re-activating stem cell markers in a subset of neurons derived from mutant progenitors. How does the proneural transcriptional switch schedule T4/T5 differentiation in Nbs?

Ato Activates Brat to Control Neuronal Commitment

As Ato is well-known to be a transcriptional activator (Aerts et al., 2010; Cachero et al., 2011), its activity is likely mediated by its target genes. To identify Ato target genes in the T4/T5 lineage, we used endogenously tagged Ato-GFP, which reproduces the expression of endogenous Ato in the IPC (Figures S4A and S4B), to perform chromatin immunoprecipitation assays using anti-GFP antibodies. The resulting list of putative Ato targets was filtered for the presence of Ato binding sites using CisTargetX (Aerts et al., 2010; Potier et al., 2012). Interestingly, among the final list of *bona fide* candidates (S2) we find the cell-fate-determinant Brat (Figure 7A), suggesting that Ato binds to brat regulatory elements *in vivo*.

Brat is a negative regulator of growth that is expressed in Nbs and is asymmetrically segregated into the GMCs in classic self-renewal divisions (Betschinger et al., 2006; Harris et al., 2011; Homem et al., 2014; Laver et al., 2015; Lee et al., 2006; Loedige

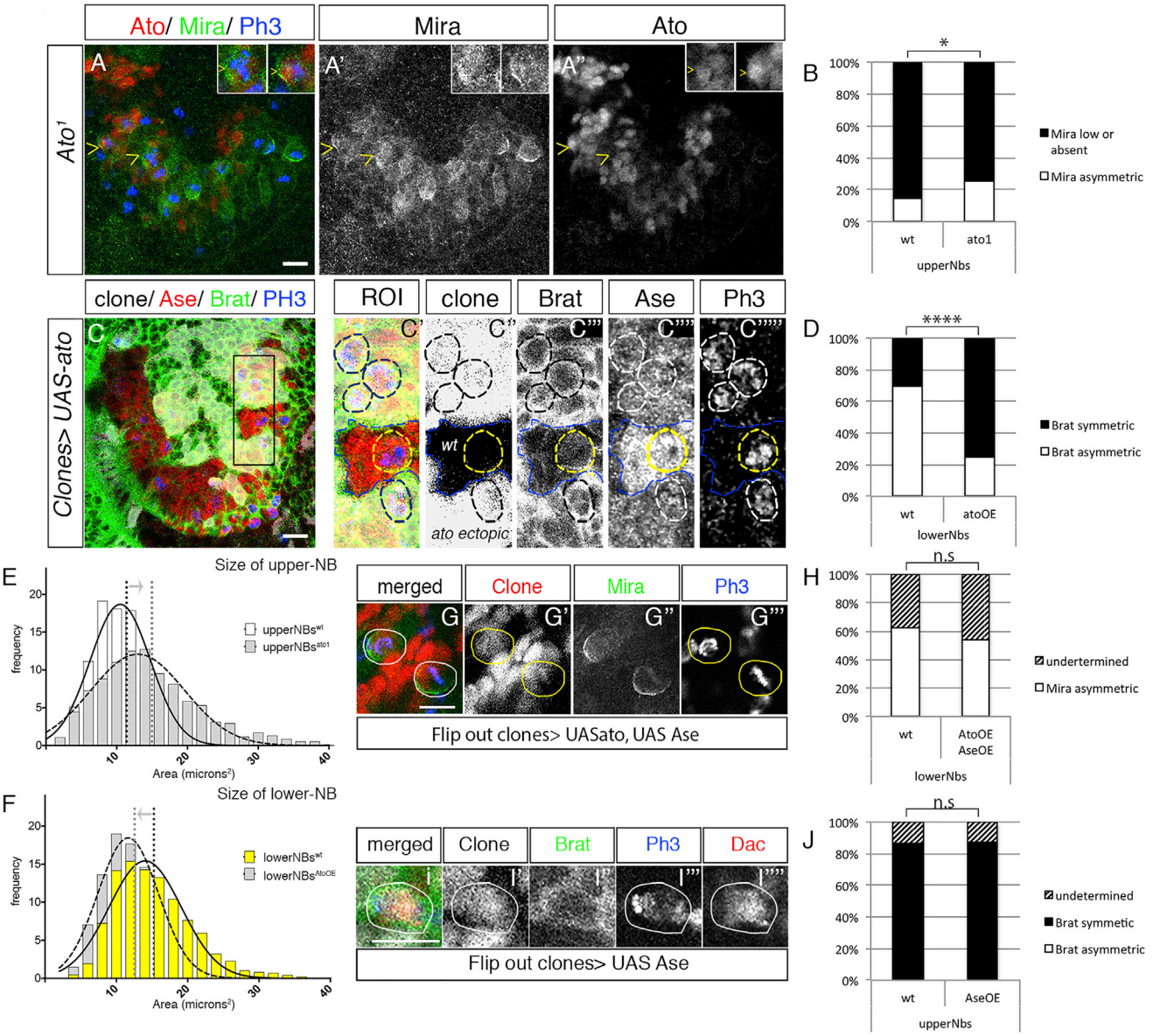

Figure 5. The Temporal Transition from Ase to Ato Controls the Onset of the Transient Amplification

(A and B) Mode of division of upper-Nbs in *ato*^{1} mutants. Localization of Mira (green) in *ato*^{1} mutant upper-Nb during mitosis. The *ato*^{1} is a point mutation and the protein can be recognized by ato antibodies. Upper-Nbs are labeled by ato (red) and mitosis by ph3 (blue). (>) Upper-Nbs in mitosis with asymmetric localization of Mira. White square, magnification of upper-Nbs with asymmetric Mira. (B) Comparison of *wt* and *ato*^{1} (*wt*: n = 28 mitosis from two samples see also Figure S1; *ato*^{1}: n = 56 mitosis from three samples; chi-square test).

(C and D) Mode of division of lower-Nbs overexpressing ato through flip-out clones. Clone is labeled with RFP (gray), lower-Nbs are labeled with Ase (red), mitosis with ph3 (blue), and the mode of division by Brat localization (green). (C'–C'''') Magnification of black square in (C). Yellow circle, *wt* lower-Nbs with asymmetric Brat (>); white circle, lower-Nbs overexpressing ato with symmetric Brat; blue line, contour of flip-out clones. (D) Comparison of *wt* and ato overexpression clones (n = 54 mitosis from three samples; chi-square test).

(E and F) Distribution of nuclear size of (E) upper-Nbs in *wt* (white, n = 1,830) and *ato*^{1} homozygous mutants (gray, n = 1,599), $p < 0.0001$ and (F) lower-Nbs in *wt* (yellow, n = 878) and ato overexpression clones (gray, n = 1,278), $p < 0.0001$. Dotted lines, mean values; arrows, swift in nuclear size. Student's t test.

(G and H) Mode of division of lower-Nbs overexpressing ato and Ase through flip-out clones (white or yellow circle). The clone is labeled with RFP (red) and lower-Nbs are identified by position and labeled with Mira (green) and mitosis with ph3 (blue). (H) Comparison of lower-Nbs in *wt* and overexpression of Ato and Ase (n = 55 mitosis from two samples; chi-square test).

(I and J) Mode of division of upper-Nbs overexpressing Ase through flip-out clones (white circle). The clone is labeled with RFP (gray), upper-Nbs are labeled with Dac (red), mitosis with ph3 (blue), and the mode of division by the differential location of Brat (green). (J) Comparison of upper-Nbs in *wt* and Ase overexpression (n = 68 mitosis from two samples; chi-square test).

*$p < 0.05$, ****$p < 0.00005$. Scale bars, 10 μm.

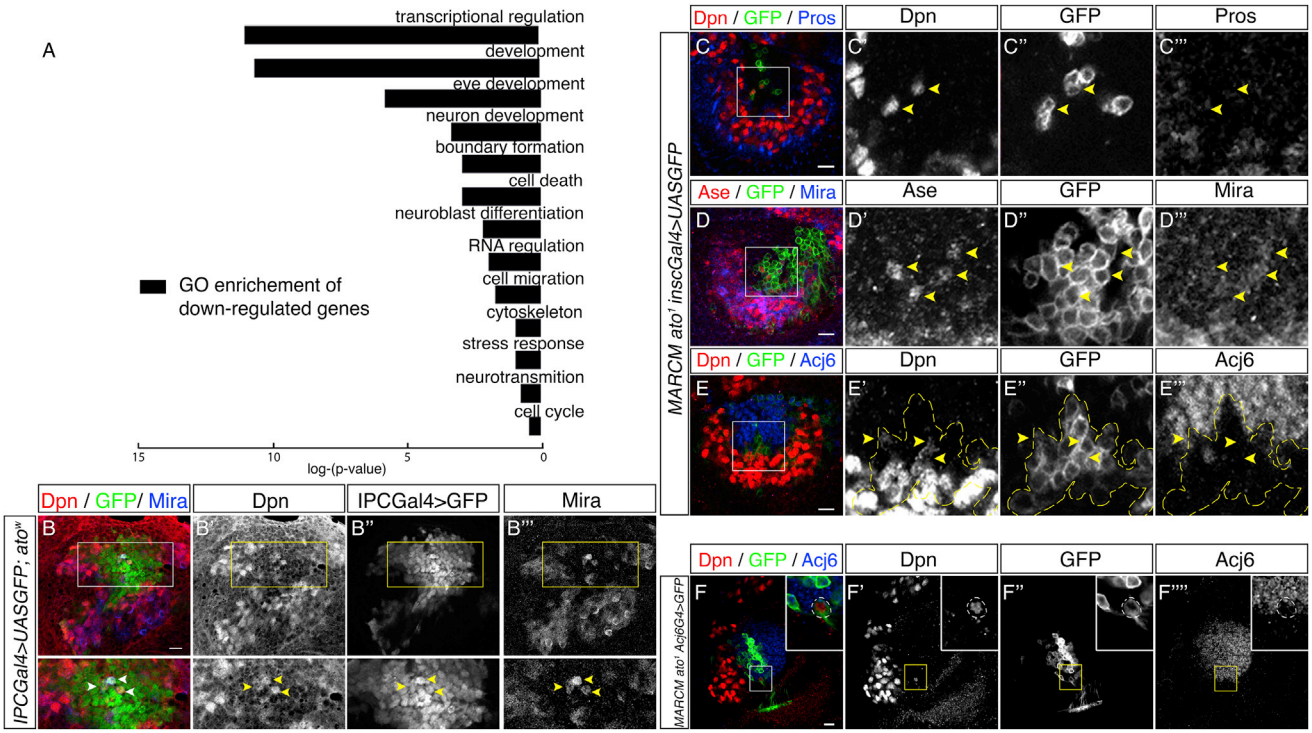

Figure 6. Ato Control of T4/T5 Differentiation

(A) Enriched gene ontology categories of genes whose expression is downregulated in T4/T5 neurons of *ato*^{1} compared with *wt*. The length of the bars indicates the fold change.

(B) Ectopic expression of Nbs markers in T4/T5 neurons of *ato*^{w} mutants. T4/T5 are labeled with GFP (green) driven by IPC-Gal4, Nbs are Dpn+ (red) and Mira+ (blue). Lower panels are magnifications of squares. Arrowheads, ectopic expression of Dpn and Mira in T4/T5.

(C–E) Ectopic expression of Nbs markers in *ato*^{1} MARCM clones. Clones are labeled with GFP driven by insc-Gal4. (C'–E') Magnification of squares in (C–E). Nbs are Dpn+ (C and C', E–E'), Ase+ (D and D'), and Mira+ (D and D'''). GMCs are Pros+ (C and C'''), and neurons Acj6+ (E and E'''). Arrowheads, ectopic expression of Nbs markers; yellow dotted line, contour of the clone.

(F) Ectopic expression of Nbs markers. Clones are labeled with GFP driven by Acj6-Gal4. Magnifications of the region of interest can be seen in every panel. Nbs are labeled with Dpn (red), neurons are labeled with Acj6 (blue) and Acj6-Gal4 reporter (green). Dotted circles, ectopic expression of Dpn in a cell with neuronal morphology (neurite) and Acj6 reporter expression (GFP).

Scale bars, 10 μm. See also Table S1.

et al., 2014; Sonoda and Wharton, 2001). Brat expression in the IPC is consistent with putative regulation by Ato (Figures 7B and 7C). Brat levels are low in Ase-expressing lower-Nbs (Figure 7C), but higher in the Ato-expressing upper-Nbs (Figure 7B). To probe the regulation of Brat expression by Ato, we first overexpressed Ato in the IPC using flip-out clones. In lower-Nbs with ectopic Ato expression (clone+, Ase+), Brat is upregulated (20% p = 0.03) (Figure 7D). Next, we generated *ato* null clones and found that the loss of Ato leads to a reduction, but not a complete loss (17% p = 0.004), of Brat in upper-Nbs when comparing *ato* null (clone −/−) with *wt* tissue (clone+/+, clone +/−) (Figure 7E). Together, these data are consistent with *Brat* being a direct target gene subject to quantitative regulation by Ato in upper-Nbs.

Next, we performed *Brat* knockdown (KD) in IPC clones using transgenic *Brat* RNAi lines. While we find no effect for *Brat* KD on the mode of upper-Nb division (Figures S4C and S4D), we find ectopic Dpn+ cells in the neuronal compartment in 60% of the brains examined (Figure 7F), a phenotype identical to that seen in *ato* loss-of-function clones in which Brat levels are reduced. Because loss of Ato reduces, but does not eliminate, Brat expression, we combined the loss of *ato* and *Brat* RNAi KD. The downregulation of *Brat* in the absence of *ato* (clone −/−) results in the ectopic expression of Dpn+ in T4/T5 neurons (Figure 7G) in 100% of the brains examined. Therefore, these data support a role for Ato-mediated upregulation of Brat in upper-Nbs that, together with its persistence at high levels in the entire T4/T5 lineage, in promoting the maintenance of a differentiated state in T4/T5 neurons.

DISCUSSION

NSC Symmetric Amplification

We report what is, to our knowledge, the first example of transient amplification by symmetric division of NSCs in a non-mammalian animal, namely the *Drosophila* fruit fly. We term these cells type III Nbs to distinguish them from previously described Nb types 0, I, and II. Embryonic NSC symmetric expansion is common in mammals, especially in gyrencephalic mammals, where oRG are highly abundant. This includes ferrets, non-human primates, and humans, but not rodents. oRG is thought to be in part responsible for the brain size expansion

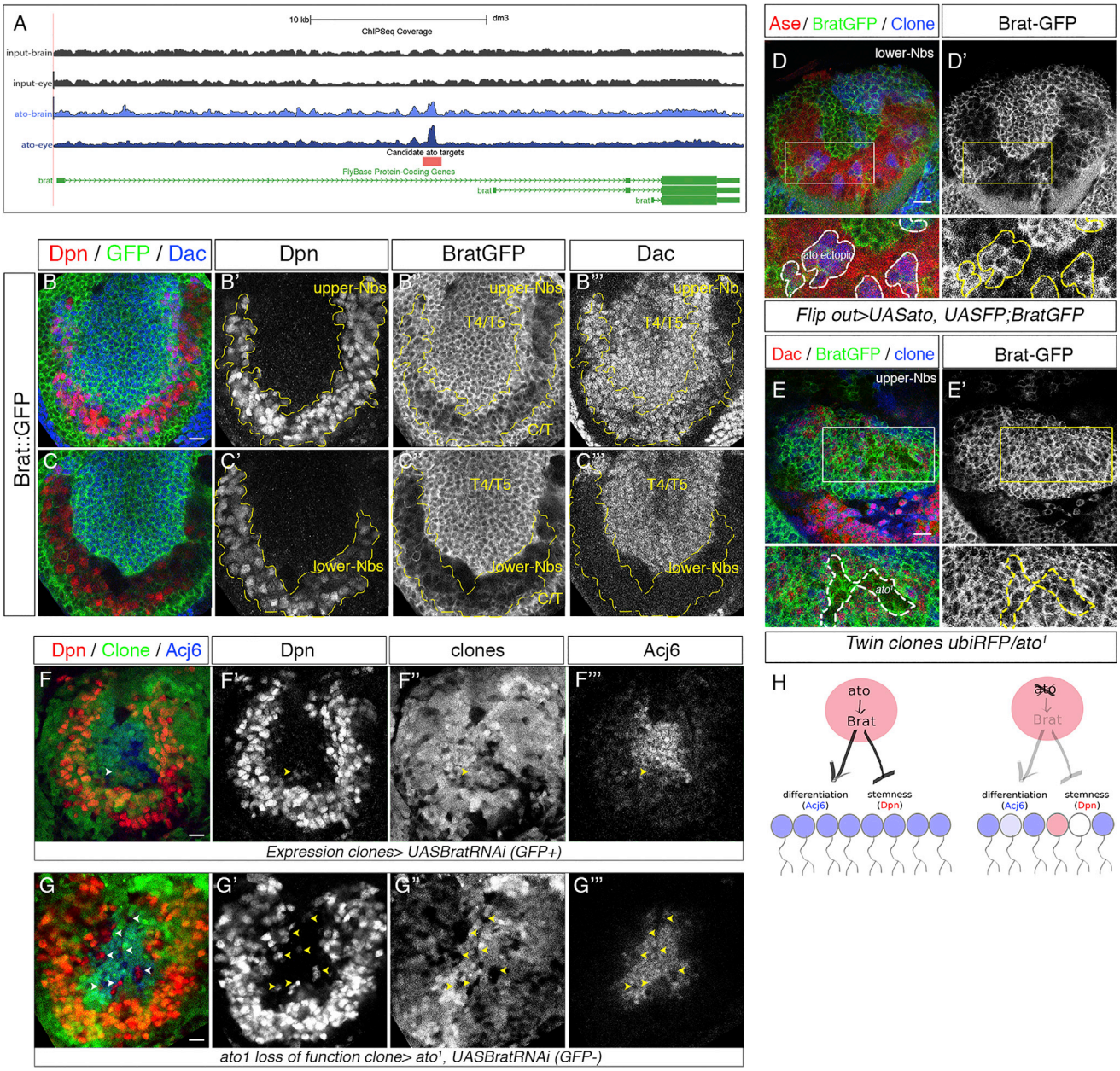

Figure 7. Brat Mediates Ato Control of Differentiation

(A) Coverage of the chromatin immunoprecipitation sequencing (Chip-seq) of Ato on the *Brat* gene (green) in brain (light blue) and eye (dark blue) samples and their respective inputs (dark gray). Red box, putative ato binding site.

(B and C) Brat endogenous expression (green) in lower-Nbs (C–C''') Dpn+ (red) and upper-Nbs (B–B''') Dpn+ (red) and Dac+ (blue). Yellow line, contour of Dpn expression.

(D) Brat expression (green) in flip-out clones (blue) overexpressing Ato. Lower-Nbs are Ase+ (red). Lower panels are magnifications of the squares in upper panels. White and yellow lines, contour of clones.

(E) Brat expression (green) in *ato*^{1} twin clones (blue). Upper-Nbs and T4/T5 neurons are Dac+ (red). Lower panels are magnifications of the squares in upper panels. White and yellow lines, contour of *ato*^{1} clones.

(F–F''') Ectopic expression of Nbs markers in flip-out clones (green) expressing Brat-RNAi. Nbs are Dpn+ (red) neurons are Acj6+ (blue). Arrowhead, ectopic expression of Nbs markers.

(G–G''') Enhanced ectopic expressions of Nbs markers in twin clones of *ato*^{1} (green −/−) and Brat-RNAi. Nbs are Dpn+ (red) neurons are Acj6+ (blue). Arrowhead, ectopic expression of Nbs markers.

(H) Mechanistic model of the role of ato in T4/T5 development. Ato activates Brat creating a quantitative change in its expression that is propagated throughout the lineage to ensure the commitment of T4/T5 neurons and the exit from stemness. In the absence of ato, Brat is downregulated leading to lack of differentiation and sporadic de-differentiation. Moreover, fewer neurons are produced due to the role of ato in symmetric division.

Scale bars, 10 μm. See also Figure S4 and Table S2.

that is observed in these species. Having simpler models that recapitulate at least some aspects of oRG biology could be particularly relevant to the study of fundamental questions surrounding the control of brain size. Understanding the symmetry of self-renewal is also relevant for the study of adult neurogenesis where symmetric division have recently been shown to be predominant (Obernier et al., 2018). In this context, limited rounds of symmetric self-renewal and consuming symmetric differentiation division can explain how neurogenesis is sustained for extended periods of time. In this work, we find that *Drosophila* symmetrically amplifying Nbs expand the progenitor pool while at the same time scheduling the future terminal differentiation of their progeny. We describe genetic and regulatory control mechanisms of these features and the consequences of interfering with such mechanisms for brain development.

Temporal Control of Lineage Size

The type III *Drosophila* Nbs described here are located in the visual system anlagen in a region known as the IPC, where they generate two different neuronal populations—the C/T and the T4/T5 neurons—in that specific temporal order. We show that IPC Nbs transit through two distinct types of proliferation: an earlier phase of type I asymmetric divisions to generate C/T neurons and a later phase of symmetric transit amplification. These two phases coincide with a change in neuronal fate and number. While late born T4/T5 constitute one of the largest lineages in the *Drosophila* brain, the early born C/T neurons are two times less abundant (Takemura et al., 2008). Although it is difficult to know the exact number of symmetric divisions each upper-Nb undergoes, it is interesting to note that one symmetric amplification before the terminal production of GMCs would account for the doubling of the number of upper-Nbs compared with lower-Nbs that we observe, resulting in exactly four T4/T5 neurons per upper-Nb. A concurrent study (Pinto-Teixeira et al., 2018) proposes that this particular stoichiometry may be accounted for through a single terminal Nb division. While our observations do not contradict the stoichiometry, the suggestion that there is no amplifying step prior to the terminal division is difficult to reconcile with the multiple lines of evidence presented here. Together with a study by Apitz and Salecker (2018), these authors further show that the layer specificity of T4/T5 neurons relies on Dpp and that the T4 versus T5 fate is Notch dependent. The Apitz and Salecker study further shows how the Dpp signal is maintained from NE progenitors to neurons through a temporal relay mechanism. Together, these studies open the door for understanding precisely how this very large and complex lineage combines numerical expansion, cell fate, and layer-specific targeting over a series of successive temporal developmental transitions.

In this study, we focus on the temporal transition of proliferation properties and show that they are regulated by the serial expression of two proneural proteins, Ase and Ato. Interestingly Ase and Ato had not been involved in C/T versus T4/T5 fate decision, suggesting that lineage size can be controlled independently of cell fate. Previous studies (Apitz and Salecker, 2015) in the IPC have shown that the switch in neuronal fate depends on another temporal series of two factors called Tailless and Dichaete. It would be interesting to investigate the crosstalk between these two temporal series as a model to further understand how neuronal numbers and neuronal fate are integrated during development. Our findings provide one of the first examples of Nbs changing their proliferation properties to achieve lineage size proportions, where NSC amplification is causally linked to an increase in the number of neurons generated.

A Dual Role: Stem Cell Amplification and Differentiation

Proneural proteins are highly conserved transcription factors that promote the transition from precursors to neurons (Bertrand et al., 2002; Parras et al., 1996). In the peripheral nervous system of *Drosophila*, Ato acts as a transcriptional activator regulating the commitment of different subsets of epithelial cells to the neuronal fate (Jarman et al., 1993, 1994). However, in the IPC Nbs, Ato plays a dual role. On the one hand, it promotes the amplification of progenitors that express it, and on the other hand it ensures the terminal differentiation of their neuronal progeny. Curiously, Atoh1, the mammalian homolog of Ato, has been described both as a tumor suppressor in colorectal cancer (Bossuyt et al., 2009; Leow et al., 2004) and as an oncogene in medulloblastoma (Ben-Arie et al., 1997; Zhao et al., 2008), the most common malignant brain tumor in children. We suspect that this context-dependent function may be related to the dual role of Ato in amplification and differentiation characterized here.

It is important to note that, in the IPC, Ato can robustly impose symmetric division when ectopically expressed. However, only a fraction of Nbs divisions are affected in its absence. This demonstrates that Ato is sufficient, but not always necessary, for symmetric division, and suggests the existence of an overlapping and independent mechanism controlling the process. Ato in this context likely acts to ensure robust transitions first to symmetric amplification and later to differentiation. We propose that the strong reduction of T4/T5 neuron numbers in *ato* mutant brains is due to an incomplete transition from asymmetric to symmetric division. However, we cannot exclude the effect of other functions of Ato yet to be characterized, for example in ensuring neuronal survival.

The fact that Ato expression in Nbs controls the differentiation of T4/T5 neurons is demonstrated by the ectopic expression of Nbs markers and the global downregulation of differentiation genes in neurons of *ato* mutant animals. This resembles the de-differentiation phenotype previously found in *Drosophila* mutants of longitudinal lacking (lola) (Southall et al., 2014). However, unlike *lola*, Ato itself is never expressed in neurons, not even transiently. We propose that a stable cellular memory of differentiation is initiated transcriptionally in stem cells and inherited through successive cell divisions to ensure terminal differentiation of neuronal progeny. What the mechanisms of such a memory are, how they are activated in stem cells, and how they relate to stem cell division mode are exciting questions for future investigation.

Quantitative Regulation and the Transcriptional Control of Developmental Time

A recurring observation throughout our analyses is that quantitative, rather than all or nothing, changes in gene expression downstream of Ato control the temporal progression of developmental events. For example, premature Ato expression causes a

relatively modest reduction in Ase expression, and yet suffices to induce symmetric division prematurely. Similarly, quantitative regulation of Brat levels is required for a dose-dependent maintenance of terminal differentiation in postmitotic neurons. Brat is a member of a family of evolutionarily conserved tumor suppressor proteins that regulate differentiation and growth (Arama et al., 2000; Frank et al., 2002; Lee et al., 2006; Sonoda and Wharton, 2001). In type I and II Nbs, Brat is asymmetrically inherited to promote differentiation (Betschinger et al., 2006; Lee et al., 2006). In IPC Nbs, Brat is symmetrically inherited during the transient amplification but it does not prevent Nb gene expression. We therefore propose that it is the progressive accumulation through temporal quantitative regulation, rather than its expression *per se*, that schedules the onset and maintenance of differentiation.

How cell division and differentiation are coordinated to determine organ size is a fundamentally important but poorly understood process. In *Drosophila*, the intrinsic activity life time of given proneural transcription factor is both a developmental (Quan et al., 2016) and evolutionary (Weinberger et al., 2017) strategy for the control of cell number in the peripheral nervous system. During the development of mammalian telencephalon, the expression of Ascl1, the mammalian homolog of *Drosophila* Achaete-scute proteins such as Ase, oscillates in NSCs. These oscillations promote proliferation, while sustained expression of Ascl1 promotes neuronal differentiation (Imayoshi et al., 2013). Finally, there is evidence that spatiotemporal transitions in cross-regulatory transcription factors control root meristem growth in plants (Scacchi et al., 2010). Here we show that a similar logic regulates brain size. These observations suggest that the differential, temporally restricted and quantitative regulation of transcription factors and their target genes may serve a universal role as molecular clocks underlying the coordinated temporal order of developmental events.

STAR★METHODS

Detailed methods are provided in the online version of this paper and include the following:

- KEY RESOURCES TABLE
- CONTACT FOR REAGENT AND RESOURCE AND SHARING
- EXPERIMENTAL MODEL AND SUBJECT DETAILS
  - Species
- METHOD DETAILS
  - Immunohistochemistry
  - Imaging
  - MARCM Clones
  - Flip-Out Clones
  - Twin Clones
  - Quantification of Different Modes of Division of IPC Nbs
  - Quantification of Intensity Levels
  - Quantification of Adult T4/T5 Neuronal Numbers
  - Profiling of Translated mRNAs
  - Chromatin Immunoprecipitation
  - Cell Size Quantification
  - Live Imaging of Brain Explants
  - Primary Cultures and Life Imaging
- QUANTIFICATION AND STATISTICAL ANALYSIS
- DATA AND SOFTWARE AVAILABILITY

SUPPLEMENTAL INFORMATION

Supplemental Information includes four figures, two tables, and three movies and can be found with this article online at https://doi.org/10.1016/j.devcel.2018.02.023.

ACKNOWLEDGMENTS

We are grateful to A. Brand, J. Knoblich, H. Bellen, F. Tejedor, C. Desplan, Y.N. Jan, the Bloomington *Drosophila* Stock Center (NIH P40OD018537), the Vienna Drosophila stock center, and the Developmental Studies Hybridoma Bank (NICHD of the NIH University of Iowa, Department of Biology, Iowa City, IA 52242) for flies, constructs, and antibodies. We acknowledge the Nucleomics core facility, Vlaams Instituut voor Biotechnologie (VIB; Flanders Institute for Biotechnology) for their sequencing services, and the scientific and technical assistance of the ICM imaging center (“Investissements d’avenir” program [ANR-10-IAIHU-06] and [ANR-11-INbS-0011]). We thank C. Desplan and Iris Salecker for helpful discussions and N. Renier, P. Vanderhaeghen, and I. Miguel-Aliaga for comments on the manuscript. This work was supported by the program “Investissements d’avenir” ANR-10-IAIHU-06, ICM, VIB, the WiBrain Interuniversity Attraction Pole network (Belspo), the Paul G. Allen Frontiers Group, a Funds for Scientific Research Flanders (Fonds Wetenschappelijke Onderzoeks; FWO) postdoctoral fellowship to N.M., a Becas Chile postdoctoral fellowship to C.O., a University of Leuven postdoctoral fellowship (PDM) to A.S., an EMBO Long-Term Fellowship and a VIB Omics postdoctoral fellowship to R.E., and a China Scholarship Council doctoral fellowship to T.T-.Z. B.A.H is an Allen Distinguished Investigator and an Einstein Fellow of the Berlin Institute of Health.

AUTHOR CONTRIBUTIONS

Conceptualization, B.A.H. and N.M.; Methodology, B.A.H. and N.M.; Software, M.F., N.M., and R.E.; Validation, M.F. and N.M.; Formal Analysis, M.F. and N.M.; Investigation, N.M., C.O., A.S., and T.-T.Z.; Resources, R.E., J.Y., A.C., and N.D.G.; Data Curation, M.F. and N.M.; Writing – Original Draft, N.M.; Writing – Review & Editing, B.A.H. and N.M.; Visualization, N.M.; Supervision, B.A.H. and N.M.; Project Administration, B.A.H. and N.M.; Funding Acquisition, B.A.H.

DECLARATION OF INTERESTS

The authors declare no competing interests.

Received: July 6, 2017
Revised: February 12, 2018
Accepted: February 26, 2018
Published: March 22, 2018

REFERENCES

Aerts, S., Quan, X.J., Claeys, A., Naval Sanchez, M., Tate, P., Yan, J., and Hassan, B.A. (2010). Robust target gene discovery through transcriptome perturbations and genome-wide enhancer predictions in drosophila uncovers a regulatory basis for sensory specification. PLoS Biol. *8*, e1000435.

Allan, D.W., and Thor, S. (2015). Transcriptional selectors, masters, and combinatorial codes: regulatory principles of neural subtype specification. Wiley Interdiscip. Rev. Dev. Biol. *4*, 505–528.

Apitz, H., and Salecker, I. (2015). A region-specific neurogenesis mode requires migratory progenitors in the *Drosophila* visual system. Nat. Neurosci. *18*, 46–55.

Apitz, H., and Salecker, I. (2018). Spatio-temporal relays control layer specificity of motion-direction sensitive neurons in *Drosophila*. BioRxiv. https://doi.org/10.1101/262451.

Arama, E., Dickman, D., Kimchie, Z., Shearn, A., and Lev, Z. (2000). Mutations in the beta-propeller domain of the *Drosophila* brain tumor (brat) protein induce neoplasm in the larval brain. Oncogene *19*, 3706–3716.

Basto, R., and Oegema, K. (2015). Methods in cell biology. Centrosome & centriole. Preface. Methods Cell Biol. *129*, xvii–xix.

Baumgardt, M., Karlsson, D., Salmani, B.Y., Bivik, C., MacDonald, R.B., Gunnar, E., and Thor, S. (2014). Global programmed switch in neural daughter cell proliferation mode triggered by a temporal gene cascade. Dev. Cell *30*, 192–208.

Behnia, R., and Desplan, C. (2015). Visual circuits in flies: beginning to see the whole picture. Curr. Opin. Neurobiol. *34*, 125–132.

Bello, B.C., Izergina, N., Caussinus, E., and Reichert, H. (2008). Amplification of neural stem cell proliferation by intermediate progenitor cells in *Drosophila* brain development. Neural Dev. *3*, 5.

Ben-Arie, N., Bellen, H.J., Armstrong, D.L., McCall, A.E., Gordadze, P.R., Guo, Q., Matzuk, M.M., and Zoghbi, H.Y. (1997). Math1 is essential for genesis of cerebellar granule neurons. Nature *390*, 169–172.

Bertrand, N., Castro, D.S., and Guillemot, F. (2002). Proneural genes and the specification of neural cell types. Nat. Rev. Neurosci. *3*, 517–530.

Betschinger, J., Mechtler, K., and Knoblich, J.A. (2006). Asymmetric segregation of the tumor suppressor brat regulates self-renewal in *Drosophila* neural stem cells. Cell *124*, 1241–1253.

Boone, J.Q., and Doe, C.Q. (2008). Identification of *Drosophila* type II neuroblast lineages containing transit amplifying ganglion mother cells. Dev. Neurobiol. *68*, 1185–1195.

Borst, A., and Helmstaedter, M. (2015). Common circuit design in fly and mammalian motion vision. Nat. Neurosci. *18*, 1067–1076.

Bossuyt, W., Kazanjian, A., Geest, N.D., Kelst, S.V., Hertogh, G.D., Geboes, K., Boivin, G.P., Luciani, J., Fuks, F., Chuah, M., et al. (2009). Atonal homolog 1 is a tumor suppressor gene. PLoS Biol. *7*, e39.

Cachero, S., Simpson, T.I., Zur Lage, P.I., Ma, L., Newton, F.G., Holohan, E.E., Armstrong, J.D., and Jarman, A.P. (2011). The gene regulatory cascade linking proneural specification with differentiation in *Drosophila* sensory neurons. PLoS Biol. *9*, e1000568.

Choi, C.M., Vilain, S., Langen, M., Kelst, S.V., Geest, N.D., Yan, J., Verstreken, P., and Hassan, B.A. (2009). Conditional mutagenesis in *Drosophila*. Science *324*, 54.

Dietzl, G., Chen, D., Schnorrer, F., Su, K.-C., Barinova, Y., Fellner, M., Gasser, B., Kinsey, K., Oppel, S., Scheiblauer, S., et al. (2007). A genome-wide transgenic RNAi library for conditional gene inactivation in *Drosophila*. Nature *448*, 151–156.

Doe, C.Q. (1996). Asymmetric cell division and neurogenesis. Curr. Opin. Genet. Dev. *6*, 562–566.

Doe, C.Q., Fuerstenberg, S., and Peng, C.Y. (1998). Neural stem cells: from fly to vertebrates. J. Neurobiol. *36*, 111–127.

Edgar, R., Domrachev, M., and Lash, A.E. (2002). Gene expression omnibus: NCBI gene expression and hybridization array data repository. Nucleic Acids Res. *30*, 207–210.

Egger, B., Boone, J.Q., Stevens, N.R., Brand, A.H., and Doe, C.Q. (2007). Regulation of spindle orientation and neural stem cell fate in the *Drosophila* optic lobe. Neural Dev. *2*, 1.

Erclik, T., Li, X., Courgeon, M., Bertet, C., Chen, Z., Baumert, R., Ng, J., Koo, C., Arain, U., Behnia, R., et al. (2017). Integration of temporal and spatial patterning generates neural diversity. Nature *541*, 365–370.

Frank, D.J., Edgar, B.A., and Roth, M.B. (2002). The *Drosophila* melanogaster gene brain tumor negatively regulates cell growth and ribosomal RNA synthesis. Development *129*, 399–407.

Fuse, N., Hisata, K., Katzen, A.L., and Matsuzaki, F. (2003). Heterotrimeric G proteins regulate daughter cell size asymmetry in *Drosophila* neuroblast divisions. Curr. Biol. *13*, 947–954.

Guillemot, F., and Hassan, B.A. (2017). Beyond proneural: emerging functions and regulations of proneural proteins. Curr. Opin. Neurobiol. *42*, 93–101.

Hansen, D.V., Lui, J.H., Parker, P.R., and Kriegstein, A.R. (2010). Neurogenic radial glia in the outer subventricular zone of human neocortex. Nature *464*, 554–561.

Harris, R.E., Pargett, M., Sutcliffe, C., Umulis, D., and Ashe, H.L. (2011). Brat promotes stem cell differentiation via control of a bistable switch that restricts BMP signaling. Dev. Cell *20*, 72–83.

Hofbauer, A., and Campos-Ortega, J.A. (1990). Proliferation pattern and early differentiation of the optic lobes in *Drosophila* melanogaster. Roux Arch. Dev. Biol. *198*, 264–274.

Homem, C.C., Reichardt, I., Berger, C., Lendl, T., and Knoblich, J.A. (2013). Long-term live cell imaging and automated 4D analysis of *Drosophila* neuroblast lineages. PLoS One *8*, e79588.

Homem, C.C.F., Steinmann, V., Burkard, T.R., Jais, A., Esterbauer, H., and Knoblich, J.A. (2014). Ecdysone and mediator change energy metabolism to terminate proliferation in *Drosophila* neural stem cells. Cell *158*, 874–888.

Huang, C., Chan, J.A., and Schuurmans, C. (2014). Proneural bHLH genes in development and disease. Curr. Top. Dev. Biol. *110*, 75–127.

Imayoshi, I., Isomura, A., Harima, Y., Kawaguchi, K., Kori, H., Miyachi, H., Fujiwara, T., Ishidate, F., and Kageyama, R. (2013). Oscillatory control of factors determining multipotency and fate in mouse neural progenitors. Science *342*, 1203–1208.

Jarman, A.P., Grau, Y., Jan, L.Y., and Jan, Y.N. (1993). Atonal is a proneural gene that directs chordotonal organ formation in the *Drosophila* peripheral nervous system. Cell *73*, 1307–1321.

Jarman, A.P., Grell, E.H., Ackerman, L., Jan, L.Y., and Jan, Y.N. (1994). Atonal is the proneural gene for *Drosophila* photoreceptors. Nature *369*, 398–400.

Kiefer, J.C., Jarman, A., and Johnson, J. (2005). Pro-neural factors and neurogenesis. Dev. Dyn. *234*, 808–813.

Lane, M.E., Sauer, K., Wallace, K., Jan, Y.N., Lehner, C.F., and Vaessin, H. (1996). Dacapo, a cyclin-dependent kinase inhibitor, stops cell proliferation during *Drosophila* development. Cell *87*, 1225–1235.

Laver, J.D., Li, X., Ray, D., Cook, K.B., Hahn, N.A., Nabeel-Shah, S., Kekis, M., Luo, H., Marsolais, A.J., Fung, K.Y., et al. (2015). Brain tumor is a sequence-specific RNA-binding protein that directs maternal mRNA clearance during the *Drosophila* maternal-to-zygotic transition. Genome Biol. *16*, 94.

Lee, C.Y., Wilkinson, B.D., Siegrist, S.E., Wharton, R.P., and Doe, C.Q. (2006). Brat is a Miranda cargo protein that promotes neuronal differentiation and inhibits neuroblast self-renewal. Dev. Cell *10*, 441–449.

Lee, T., Winter, C., Marticke, S.S., Lee, A., and Luo, L. (2000). Essential roles of *Drosophila* RhoA in the regulation of neuroblast proliferation and dendritic but not axonal morphogenesis. Neuron *25*, 307–316.

Leow, C.C., Romero, M.S., Ross, S., Polakis, P., and Gao, W.Q. (2004). Hath1, down-regulated in colon adenocarcinomas, inhibits proliferation and tumorigenesis of colon cancer cells. Cancer Res. *64*, 6050–6057.

Li, S., Wang, H., and Groth, C. (2014). *Drosophila* neuroblasts as a new model for the study of stem cell self-renewal and tumour formation. Biosci. Rep. *34*, https://doi.org/10.1042/BSR20140008.

Loedige, I., Stotz, M., Qamar, S., Kramer, K., Hennig, J., Schubert, T., Löffler, P., Längst, G., Merkl, R., Urlaub, H., and Meister, G. (2014). The NHL domain of BRAT is an RNA-binding domain that directly contacts the hunchback mRNA for regulation. Genes Dev. *28*, 749–764.

Lui, J.H., Hansen, D.V., and Kriegstein, A.R. (2011). Development and evolution of the human neocortex. Cell *146*, 18–36.

Maurange, C., Cheng, L., and Gould, A.P. (2008). Temporal transcription factors and their targets schedule the end of neural proliferation in *Drosophila*. Cell *133*, 891–902.

Miyata, T., Kawaguchi, A., Okano, H., and Ogawa, M. (2001). Asymmetric inheritance of radial glial fibers by cortical neurons. Neuron *31*, 727–741.

Nériec, N., and Desplan, C. (2016). From the eye to the brain: development of the *Drosophila* visual system. Curr. Top. Dev. Biol. *116*, 247–271.

Ngo, K.T., Wang, J., Junker, M., Kriz, S., Vo, G., Asem, B., Olson, J.M., Banerjee, U., and Hartenstein, V. (2010). Concomitant requirement for Notch

and Jak/Stat signaling during neuro-epithelial differentiation in the *Drosophila* optic lobe. Dev. Biol. *346*, 284–295.

Ngo, K.T., Andrade, I., and Hartenstein, V. (2017). Spatio-temporal pattern of neuronal differentiation in the *Drosophila* visual system: a user's guide to the dynamic morphology of the developing optic lobe. Dev. Biol. *428*, 1–24.

Noctor, S.C., Martínez-Cerdeño, V., Ivic, L., and Kriegstein, A.R. (2004). Cortical neurons arise in symmetric and asymmetric division zones and migrate through specific phases. Nat. Neurosci. *7*, 136–144.

Obernier, K., Cebrian-Silla, A., Thomson, M., Parraguez, J.I., Anderson, R., Guinto, C., Rodriguez, J.R., Garcia-Verdugo, J.M., and Alvarez-Buylla, A. (2018). Adult neurogenesis is sustained by symmetric self-renewal and differentiation. Cell Stem Cell *22*, 221–234.e8.

Oliva, C., Choi, C.M., Nicolai, L.J., Mora, N., De Geest, N., and Hassan, B.A. (2014). Proper connectivity of *Drosophila* motion detector neurons requires Atonal function in progenitor cells. Neural Dev. *9*, 4.

Parras, C., García-Alonso, L.A., Rodriguez, I., and Jiménez, F. (1996). Control of neural precursor specification by proneural proteins in the CNS of *Drosophila*. EMBO J. *15*, 6394–6399.

Pérez-Lluch, S., Blanco, E., Carbonell, A., Raha, D., Snyder, M., Serras, F., and Corominas, M. (2011). Genome-wide chromatin occupancy analysis reveals a role for ASH2 in transcriptional pausing. Nucleic Acids Res. *39*, 4628–4639.

Pinto-Teixeira, F., Koo, C., Rossi, A.M., Neriec, N., Bertet, C., Li, X., Del-Valle-Rodriguez, A., and Desplan, C. (2018). Development of concurrent retinotopic maps in the fly motion detection circuit. Cell. https://doi.org/10.1016/j.cell.2018.02.053.

Potier, D., Atak, Z.K., Sanchez, M.N., Herrmann, C., and Aerts, S. (2012). Using cisTargetX to predict transcriptional targets and networks in *Drosophila*. Methods Mol. Biol. *786*, 291–314.

Quan, X.J., Yuan, L., Tiberi, L., Claeys, A., De Geest, N., Yan, J., van der Kant, R., Xie, W.R., Klisch, T.J., Shymkowitz, J., et al. (2016). Post-translational control of the temporal dynamics of transcription factor activity regulates neurogenesis. Cell *164*, 460–475.

Reillo, I., and Borrell, V. (2012). Germinal zones in the developing cerebral cortex of ferret: ontogeny, cell cycle kinetics, and diversity of progenitors. Cereb. Cortex *22*, 2039–2054.

Scacchi, E., Salinas, P., Gujas, B., Santuari, L., Krogan, N., Ragni, L., Berleth, T., and Hardtke, C.S. (2010). Spatio-temporal sequence of cross-regulatory events in root meristem growth. Proc. Natl. Acad. Sci. USA *107*, 22734–22739.

Shearin, H.K., Macdonald, I.S., Spector, L.P., and Stowers, R.S. (2014). Hexameric GFP and mCherry reporters for the *Drosophila* GAL4, Q, and LexA transcription systems. Genetics *196*, 951–960.

Sonoda, J., and Wharton, R.P. (2001). *Drosophila* brain tumor is a translational repressor. Genes Dev. *15*, 762–773.

Southall, T.D., Davidson, C.M., Miller, C., Carr, A., and Brand, A.H. (2014). Dedifferentiation of neurons precedes tumor formation in lola mutants. Dev. Cell *28*, 685–696.

Stahl, R., Walcher, T., De Juan Romero, C., Pilz, G.A., Cappello, S., Irmler, M., Sanz-Aquela, J.M., Beckers, J., Blum, R., Borrell, V., and Götz, M. (2013). Trnp1 regulates expansion and folding of the mammalian cerebral cortex by control of radial glial fate. Cell *153*, 535–549.

Takemura, S., Lu, Z., and Meinerzhagen, I.A. (2008). Synaptic circuits of the *Drosophila* optic lobe: the input terminals to the medulla. J. Comp. Neurol. *509*, 493–513.

Takemura, S.Y., Nern, A., Chklovskii, D.B., Scheffer, L.K., Rubin, G.M., and Meinertzhagen, I.A. (2017). The comprehensive connectome of a neural substrate for "ON" motion detection in *Drosophila*. Elife *6*, https://doi.org/10.7554/eLife.24394.

Taverna, E., Götz, M., and Huttner, W.B. (2014). The cell biology of neurogenesis: toward an understanding of the development and evolution of the neocortex. Annu. Rev. Cell Dev. Biol. *30*, 465–502.

Thomas, A., Lee, P.J., Dalton, J.E., Nomie, K.J., Stoica, L., Costa-Mattioli, M., Chang, P., Nuzhdin, S., Arbeitman, M.N., and Dierick, H.A. (2012). A versatile method for cell-specific profiling of translated mRNAs in *Drosophila*. PLoS One *7*, e40276.

Weinberger, S., Topping, M.P., Yan, J., Claeys, A., Geest, N.D., Ozbay, D., Hassan, T., He, X., Albert, J.T., Hassan, B.A., and Ramaekers, A. (2017). Evolutionary changes in transcription factor coding sequence quantitatively alter sensory organ development and function. Elife *6*, https://doi.org/10.7554/eLife.26402.

Wodarz, A., and Huttner, W.B. (2003). Asymmetric cell division during neurogenesis in *Drosophila* and vertebrates. Mech. Dev. *120*, 1297–1309.

Zhao, H., Ayrault, O., Zindy, F., Kim, J.H., and Roussel, M.F. (2008). Post-transcriptional down-regulation of Atoh1/Math1 by bone morphogenic proteins suppresses medulloblastoma development. Genes Dev. *22*, 722–727.

Zhong, W., and Chia, W. (2008). Neurogenesis and asymmetric cell division. Curr. Opin. Neurobiol. *18*, 4–11.

STAR★METHODS

KEY RESOURCES TABLE

REAGENT or RESOURCE	SOURCE	IDENTIFIER
Antibodies		
Guinea pig anti-Ase (1:100)	Laboratory of J.Knoblich	RRID: AB_2567568
Sheep anti-Ato (1:250)	Laboratory of A. Jarman	RRID: AB_2568143
Guinea pig anti-Dpn (1:10000)	Laboratory of A.Brand	N/A
Guinea pig anti-Dpn (1:300)	Laboratory of C.Desplan	N/A
Rabbit anti-Mira (1:100)	Laboratory of Y.N.Jan	RRID: AB_2569537
Rat anti-Elav (1:100)	DSHB	Cat# 7E8A10; RRID: AB_528218
Mouse anti-pros (1:4)	DSHB	Cat# MR1A; RRID: AB_2569636
Rabbit anti-pH3-ser10 (1:500)	Millipore	Cat# 06-570; RRID: AB_310177
Rat anti-ph3-ser28 (1:100)	Abcam	Cat# Ab10543; RRID: AB_2295065
Mouse anti-Dac (1:50)	DSHB	Cat# mAbbdac2-3; RRID: AB_528190
Mouse anti-Dap (1:100)	DSHB	Cat# NP1; RRID: AB_10805540
Mouse anti Acj6 (1:10)	DSHB	Cat# Acj6; RRID: AB_528067
Rabbit anti-betaGal (1:1000)	MP Biomedicals/Cappel	Cat# 0855976; RRID: AB_2334934
Rabbit anti-GFP-Chip Grade (1:1000)	Abcam	Cat# Ab290; RRID: AB_2313768
rabbit anti-GFP(1:1000)	Milipore	Cat# 06-896; RRID: AB_11214044
Anti-GFP V_HH coupled to magnetic microparticles	Chromoteck	Cat# GFP-Trap_M; RRID: AB_2631359
Secondary antibodies conjugated with Alexa 488, Alexa55, Alexa647 and Alexa405	Invitrogen	N/A
Chemicals, Peptides, and Recombinant Proteins		
Schneider's Drosophila Medium	Gibco	21720-024
Insulin	Sigma-Aldrich	I0516
20-hydroxyecdysone	Sigma-Aldrich	5289-74-7
FBS, heat inactivated	Sigma-Aldrich	F4135
Anti-GFP V_HH coupled to magnetic microparticles	Chromoteck	GFP-Trap_M
Oil 10 S Voltalef	VWR	24627.188
KIT DE MEMBRANE STANDARD ET KCl.	System-c-industrie	5775/098094
Laminin	Sigma-Aldrich	Cc095
Poly-d-lysine-hydobromide	Sigma-Aldrich	P6282
l-glutamate	Sigma-Aldrich	G6013
Glutamine	Sigma-Aldrich	G7513
Collagenase I	Sigma-Aldrich	C2674
Papain	Sigma-Aldrich	P4762
NaCl	Sigma-Aldrich	S3014
KCl	Sigma-Aldrich	P9541
NaH2PO4	Sigma-Aldrich	S9638
Na2HPO4	Sigma-Aldrich	S3264
NaHCO3	Sigma-Aldrich	S5761
Glucose	Sigma-Aldrich	G0350500
Deposited Data		
Translatome t4/t5 neurons	This study	GEO: GSE110705
Brain chip	This study	GEO: GSE110687
Experimental Models: Organisms/Strains		
D.melanogaster: *Canton Special*	Laboratory of B.Hassan	N/A
D.melanogaster: *w;ato-lacZ;*	Laboratory of B.Hassan	N/A

(*Continued on next page*)

Continued		
REAGENT or RESOURCE	SOURCE	IDENTIFIER
D.melanogaster: w;act-FRT-y+-FRT-Gal4,UAS-GFP;/ST	Laboratory of B.Hassan	N/A
D.melanogaster: ;;FRT82B,ato^{1}	Laboratory of B.Hassan	N/A
D.melanogaster: ;;ato^{1}	Laboratory of B.Hassan	N/A
D.melanogaster: ;IPC-Gal4;	Laboratory of B.Hassan	N/A
D.melanogaster: ;;ato^{w}	Laboratory of B.Hassan	N/A
D.melanogaster: ;;FRT82B,ato^{1},actGal4	Laboratory of B.Hassan	N/A
D.melanogaster: ;;tubGal4,FRT82B/TM6c	Laboratory of B.Hassan	N/A
D.melanogaster: hsFlp,UAS::CD8::GFP;;FRT82B,Gal80	Laboratory of B.Hassan	N/A
D.melanogaster: ;IPC-Gal4,UAS-GFP;FRT82B,ato^{1}	Laboratory of B.Hassan	N/A
D.melanogaster: ;;UAS-Ato/TM3	Laboratory of B.Hassan	N/A
D.melanogaster: ;Ase-gal4/Cyo;	Laboratory of J. Knoblich	N/A
D.melanogaster: ;Dpn-GFP/Cyo;	Laboratory of H. Bellen lab	Mimic line *MI00051*
D.melanogaster: ;Brat-GFP;	Laboratory of H. Bellen lab	Mimic line MI02407
D.melanogaster: ;UAS-Ase;	Laboratory of F. Tejedor	N/A
D.melanogaster: Ase-Gal4	Bloomington stock center	BL45445
D.melanogaster: w;;act-FRT-cd2-FRT-gal4,UASRFP/TM3	Bloomington stock center	BL30558
D.melanogaster: ;;FRT82B,ubiRFP	Bloomington stock center	BL 30555
D.melanogaster: Acj6Gal4/FM7;;	Bloomington stock center	BL76047
D.melanogaster: ;inscGal4;	Bloomington stock center	BL8751
D.melanogaster: ;UAS-Brat-RNAi	Vienna stock center	*KK105054*
D.melanogaster: ;UAS-Rpl10Ab-GFP;	Laboratory of M.N. Arbeitman	N/A
D.melanogaster: ;UASnumb-GFP;	Bloomington stock center	N/A
D.melanogaster: ;;ato-mCherry	This study	N/A
D.melanogaster: ;;ato-GFP	This study	N/A
D.melanogaster: IPC-5xmCherry;;	This study	N/A
Software and Algorithms		
Prism 7	Graphpad	N/A
Ilastik	Open source	N/A
Fiji	Open source	N/A

CONTACT FOR REAGENT AND RESOURCE AND SHARING

Further information and requests for resources and reagents should be directed to and will be fulfilled by the Lead Contact, Bassem A. Hassan (bassem.hassan@icm-institute.org).

EXPERIMENTAL MODEL AND SUBJECT DETAILS

Species

Drosophila melanogaster

Fly stocks were cultured on standard fly food. All experiments were performed in temperature-controlled incubators at 25°C. The precise stage, either larva L3, white pupae or adults, used in each experiment is indicated in the corresponding methods section. Males and females were used indistinctly unless indicated otherwise in the method section. The fly strains used in this study were: *CS; w;ato-lacZ; w;act-FRT-y+-FRT-Gal4,UAS-GFP;/ST ;;FRT82B,ato^{1} ;IPC-Gal4; hsFlp,UAS::CD8::GFP;; FRT82B,Gal80 ;;ato^{1} ;;ato^{w} ;;FRT82B,ato^{1},actGal4, ;;tubGal4,FRT82B/TM6c, IPC-Gal4,UAS-GFP;FRT82B,ato^{1} ;Ase-gal4/Cyo; (J. Knoblich) ;Dpn-GFP/Cyo; (mimic line from H. Bellen, MI00051), ;Brat-GFP;* (mimic line from H. Bellen MI02407), ;UAS-Ase; (from F. Tejedor) *;;UAS-Ato/TM3*, Ase-Gal4 (from Bloomington stock center, BL45445), *w;;act-FRT-cd2-FRT-gal4,UASRFP/TM3* (BL30558) *;;FRT82B,ubiRFP* (BL 30555) *Acj6Gal4/FM7;;* (BL76047) *;inscGal4;* (BL8751) *;UAS-Brat-RNAi;(Vienna stock center KK105054,* Dietzl et al., 2007) (Vienna stock center KK105054,) *;UAS-Rpl10Ab-GFP;* (M.N. Arbeitman). The imago lines: *;;ato-mCherry, and ;;ato-GF,P* where generated for this project using published protocols (Choi et al., 2009). The fluorescent T4/T5 linage tracer line was constructed by the fusion of the IPC enhancer of atonal (Oliva et al., 2014) and 5 copies in tandem of the fluorescent protein mCherry with a membrane tag. The tandem was generated using published protocols (Shearin et al., 2014).

METHOD DETAILS

Immunohistochemistry

Third instar larval brains were dissected in PBS and fixed in PBT 4% formaldehyde for 15 min. Fixed brains were washed three times for 15 in PBT and incubated with the PAXDG buffer (PBT, 5% normal goat serum, 1% BSA, 0.3% deoxycholate) or PBT-BSA 1% (for Ato antibodies), for 30 min to 1hr at room temperature. Primary antibody incubation was done in PAXDG overnight at 4°C. Then the samples were washed three times with PBT and incubated with the appropriate secondary antibody in PAXDG for 2 to 3 hr, washed with PBT and mounted using the Vectashield mounting medium (Vector, Burlingame, CA, USA). The following antibodies were used Guinea pig anti-Ase (1:100, J. Knoblich), sheep anti-Ato (1:250 A. Jarman), guinea pig anti-Dpn (1:10000, A. Brand), guinea pig anti-Dpn (1:300, F. Pinto), Rabbit anti-Mira (1:100 Y.N. Jan), Rat anti-Elav (1:100, Hybridoma bank), mouse anti-pros (1:4, Hybridoma bank), Rabbit anti-pH3 (1:500, Millipore), Rat anti-ph3(1:100, Abcam), mouse anti-Dac (1:50, Hybridoma bank), mouse anti Acj6 (1:10, hybridoma bank), rabbit anti-betaGal (1:1000, Cappel), Rabbit anti-GFP (1:1000, Millipore). Secondary antibodies conjugated with Alexa 488, Alexa 555 and Alexa 647 and Alexa 405 were obtained from Invitrogen and used at 1:500.

Imaging

Imaging was performed using a Nikon A1-R confocal (Nikon, Tokyo, Japan) mounted on a Nikon Ti-2000 inverted microscope (Nikon) equipped with 405-, 488-, 561- and 639-nm lasers from Melles Griotconfocal, and an inverted Leica DMi8 equiped with HyD GaAsP ultrasensitive detectors and 405, 448, 488, 552, 638 –nm lasers. Images were processed using the ImageJ software (National Institutes of Health, Bethesda, MD, USA). Figures were prepared using Adobe Photoshop (Adobe, San Jose, CA, USA).

MARCM Clones

To follow the linage of IPC neuroblast (Nbs), females with the genotype *hsFlp,UAS::CD8::GFP;;FRT82B,tub-Gal80/TM6c* were crossed with males *;;tubGal4,FRT82B/TM6*. Second instar larvae from this cross were heat shock at 37°C for 3 hours to induce mitotic recombination, then dissect at third instar larval stage.

To study the *ato*^{1} phenotype on the differentiation of T4/T5 neurons, females with the genotype *hsFlp,UAS::CD8::GFP;;FRT82B, tub-Gal80/TM6c* were crossed with males *InscGal4;FRT82Bato*^{1}*/TM6c* or *Acj6Gal4;;FRT82Bato*^{1}*/TM6c*. Second instar larvae from these crosses were heat shock at 37°C for 3 hours to induce mitotic recombination, then dissect at third instar larval stage.

Flip-Out Clones

To study the effect of Ato and of Ase overexpression females with the genotype *hsFlp;;act-FRT-cd2-FRT-Gal4,UASRFP* were crossed with males *;BratGFP;UASato or ;BratGFP;UASAse*. Second instar larvae from this crosses were heat shock at 37°C for 15 minutes to induce recombination, then dissect at third instar larval stage. To study the effect of overexpression of Ase and Ato together and Brat downregulation, females with the genotype *hsFlp;;act-FRT-cd2-FRT-Gal4,UASRFP* were crossed with males ;UASAse;UASAto or *;BratRNAi;* respectively. Second instar larvae from this crosses were heat shock at 37°C for 15 minutes to induce recombination, then dissect at third instar larval stage.

Twin Clones

To compare the production of T4/T5 neurons in *wt* or *ato* mutant conditions, females with the genotype *hsFlp;;FRT82BubiRFP* were crossed with males *;IPCGal4,UASGFP;FRT82Bato*^{1}*/TM6c*. Second instar larvae from this cross were heat shock at 37°C for 3 hours to induce mitotic recombination, then dissect at third instar larval stage and immunoassayed. The total number of T4/T5 neurons (GFP+) that come from ato mutants (RFP-/-) or wild-type (RFP+/+) Nbs was counted for every section of the Z-stack using the Cell counter of ImageJ. The data obtained from 32 optic lobes (neurons counted=58.298) was analyzed with Graphpad in two ways: paired and unpaired T-test. To assay the expression of Brat in the absence of Ato, females with the genotype *hsFlp;;FRT82BubiRFP* were crossed with males *Brat-GFP;FRT82Bato*^{1}. Second instar larvae from this cross were heat shock at 37°C for 3 hours to induce mitotic recombination, then dissect at third instar larval stage and immunoassayed. To study the additive effect of brat downregulation in the absence of ato, females with the genotype *yhsFLP;;FRT82Bato*^{1}*actGal4* were crossed with males *;BratRNAi; FRT82BubiRFP*. Second instar larvae from this cross were heat shock at 37°C for 3 hours to induce mitotic recombination, then dissect at third instar larval stage and immunoassayed.

Quantification of Different Modes of Division of IPC Nbs

To calculate de percentage of the different modes of divisions (asymmetric vs symmetric) of IPC Nbs we manually count, with the help of the cell-counter plugging of imageJ, the differential localization of the markers Pros, Mira or Brat in mitosis. When we use Pros we distinguish between Pros in the cortex (only one pole) and no cortical location with low or absent levels in the cytoplasm. For Miranda we distinguish between Miranda in the cortex (only one pole) and Miranda low or absent in the cytoplasm. For Brat we distinguish between Brat asymmetric in the cortex (only in one pole), or Brat symmetric in the cortex (covering the whole membrane). For some mitotic cells the distribution of the marker was not clear and that mitosis was classified as undetermined.

Quantification of Intensity Levels

To quantify the effect of *ato*^{1} loss of function clones on Brat levels and of Ato overexpression on the levels of Brat and Ase we measured the mean intensity of our immunostaings using imageJ software. First we defined a Region of interest (ROI) including the clone and surrounding wild-type tissue. Then we apply a threshold to convert the signal of the clone on a binary mask and we divide the previous ROI in two areas; one positive for the clone and one negative. We measure the mean intensity of Brat and Ase in the two areas and calculate the ratio. To test the significance of the difference we performed paired t-test of ratios using graphpad.

Quantification of Adult T4/T5 Neuronal Numbers

The number of T4/T5 neurons that express the Acj6 marker in adult brains of female flies of *wild-type*, *GMR-hid* and *ato*^{1} mutants genotypes was estimated using computational segmentation. The segmentation was performed using machine-learning algorithms provided by Ilastik. The objects obtained with Ilastik software were further process using ImageJ 3D watershed-split and finally counted using the ImageJ 3D object counter. The number of T4/T5 neurons that express UAS-GFP under the control of the IPC-Gal4 driver in *GMR-hid* and *ato*^{w} mutants was estimated through a manual counting of objects per Z-section helped by the cell-counter plugging of ImageJ. It is important to notice that one cell appears in different z-sections; therefore our manual quantification is an overestimation of the number of neurons.

Profiling of Translated mRNAs

Females with the genotype *;UASRpl10Ab-GFP;* were crossed with males *;IPCgal4;* or *;IPCgal4;ato*^{1} to express the ribosomal protein Rbp10Ab tagged with GFP in T4/T5 neurons. 500 *wt* and *ato*^{1} mutant L3 brains were dissected and immunoprecipitated with antibodies against GFP (GFP-Trap, M. Chromotek). The RNA fraction bound to Rbp10Ab::GFP was then purified and sequenced following previously published protocols (Thomas et al., 2012). We compared the profiles of *wt* and *ato*^{1} mutants and obtained a list of genes that were differentially expressed over 1.5- or 2.0-fold in the mutants compared to the reference strain (FDR-corrected $P<0.05$). 2.0-fold downregulated genes where used in Gene Ontology. Raw and normalized data are deposited in the Gene Expression Omnibus (GEO) database [http://www.ncbi.nlm.nih.gov/projects/geo/] with the accession number GSE110705.

Chromatin Immunoprecipitation

400 brains were isolated from *w; ato*<atoGFP> third-instar larvae. Then, they were immunoprecipitated with anti-GFP (ab290, Abcam) purified and sequenced following previously published protocols (Pérez-Lluch et al., 2011). We obtained a list of regions with putative ato binding sites. To narrow the list to bona fide targets we filtered the list using CistargetX (Potier et al., 2012). Raw data of brain samples is deposited in the Gene Expression Omnibus (GEO) database [http://www.ncbi.nlm.nih.gov/projects/geo/] with the accession number GSE110687.

Cell Size Quantification

White pupae brains of *wild-type* and *ato*^{1} mutants where immunoassayed with antibodies against Dpn and Dac. The nucleus of all Nbs (Dpn+) was manually segmented in the images obtained. Nbs were then classified by the differential expression of Dpn and Dac: lower-Nbs (Dpn+, Dac-), upper-Nbs (Dpn+, Dac+)($n^{\text{lower-Nbs}}$=711 cells, $n^{\text{upper-Nbs}}$=878 cells, $n^{\text{upper-Nbs in ato1}}$=1278). The area of the nucleus was measured with imageJ. The data obtained was use in GraphPad for unpaired t-test statistical analysis. To study the effect of ato overexpression on the size of lower-Nbs, females with the genotype *hsFlp;act-FRT-y+-FRT-Gal4,UASGFP;* were crossed with males *;;UASato*. Second instar larvae from this cross were heat shocked at 37°C for 15 minutes to induce recombination, then dissect and immunoassayed at third instar larval stage. The nucleus of all cells expressing Ase was manually segmented. Wild-type lower-Nbs (GFP-) and lower-Nbs overexpressing Ato (GFP+) were then classified by the differential expression of GFP (n^{WT}=1830cells, n^{atoOE}=1599cells). The area of the nucleus was measured with imageJ. The data obtained was use in GraphPad for unpaired t-test statistical analysis.

Live Imaging of Brain Explants

Brains of Ipc-5xCherry ;Dpn-GFP; third-instar larvae were dissect in PBS and transfer to a bottom-glass dish with a drop of Schneider's *Drosophila* medium supplemented with 10% heat-inactivated fetal bovine serum, penicillin (100 units ml−1) and streptomycin (100 μg ml−1). The drop was then covered with a membrane permeable to oxygen and sealed with Voltalef to avoid evaporation (Basto and Oegema, 2015). The brains in culture were imaged using a Yokogawa Confocal Spinning Disk module associated to an Leica DMi8 inverted microscope taking stacks of 21 images (1 per micron) in 6 min intervals over the course of 13 hours.

Primary Cultures and Life Imaging

10 third-instar larvae of *;Brat-GFP;ato-mCherry* were cleaned in 70% ethanol for 1 minute and then dissect in supplemented Schneider's medium (10% fetal bovine serum, 2% Pen/Strep). The brains were collected and washed in Rinaldini solution (1× Rinaldini's solution: 800 mg of NaCl, 20 mg of KCl, 5 mg of NaH2PO4, 100 mg of NaHCO3 and 100 mg of glucose in 100 ml of distilled H2O; filter-sterilize the solution using the Millipore Steriflip. Rinaldini's solution can be prepared as a 10× solution and stored at 4°C for at least 3 months). Once all the brains were collected they were incubated at 30 degrees with 1 mg/ml collagenase I and 1mg/ml of papain in Schneider's solution. After 1 hour of incubation the brains were rinsed twice with Rinaldini's solution and twice

with Schneider's medium. On the last Schneider wash (200 microliters) the brains were mechanically disrupt by absorbing the liquid up and down with a pipet. The disaggregated cells were then plated in a bottom glass dish, previously coated with laminin and poly-D-lysine, and let to settle for an hour at room temperature. 3ml of primary cell culture Schneider's medium (10% fetal bovine serum, 2% Pen/Strep, L-Glutamine 20 mM, L-Glutathione 5μg/ml, Insulin 20 μg/ml, Ecdysone 5μg/ml, Schneider's medium) was add to the culture before imaging. (Homem et al., 2013). The images were taken using a Nikon A1-R confocal (Nikon, Tokyo, Japan) mounted on a Nikon Ti-2000 inverted microscope (Nikon). One image was taken every 5, 10 or 12 minutes.

QUANTIFICATION AND STATISTICAL ANALYSIS

Prism 7 (Graphpad) was used for the statistical analyses. The replicates and tests of each experiment are specified in the corresponding figure legend. When a result is mentioned but is not graphically supported the statistics are also mentioned in text and/or in the corresponding Method Details.

DATA AND SOFTWARE AVAILABILITY

The accession number for the sequencing of transtaled-RNA in t4/t5 neurons reported in this paper is GSE110705 (https://www.ncbi.nlm.nih.gov/geo/query/acc.cgi?acc= GSE110705). The accesion number for the Chip-sequencint of Atonal-GFP in L3 Brains reported in this papaer is GSE110687 (https://www.ncbi.nlm.nih.gov/geo/query/acc.cgi?acc= GSE110687) (Edgar et al., 2002).